Design, fabrication and evaluation of a Quad-Finger multimodal vibration energy harvester utilizing MFC generators

Mechanics of Advanced Materials and Structures

ISSN: 1537-6494 (Print) 1537-6532 (Online) Journal homepage: www.tandfonline.com/journals/umcm20

Design, fabrication and evaluation of a Quad-Finger multimodal vibration energy harvester utilizing MFC generators

M. Askari, M. Ghandchi Tehrani, E. Brusa, A. Carrera & C. Delprete

To cite this article: M. Askari, M. Ghandchi Tehrani, E. Brusa, A. Carrera & C. Delprete (2026) Design, fabrication and evaluation of a Quad-Finger multimodal vibration energy harvester utilizing MFC generators, Mechanics of Advanced Materials and Structures, 33:1, 2465911, DOI: 10.1080/15376494.2025.2465911

To link to this article: https://doi.org/10.1080/15376494.2025.2465911

MECHANICS OF ADVANCED MATERIALS AND STRUCTURES
2026, VOL. 33, NO. 1, 2465911
https://doi.org/10.1080/15376494.2025.2465911

Taylor & Francis
Taylor & Francis Group

ORIGINAL ARTICLE

Design, fabrication and evaluation of a Quad-Finger multimodal vibration energy harvester utilizing MFC generators

M. Askari[a], M. Ghandchi Tehrani[a], E. Brusa[b], A. Carrera[b], and C. Delprete[b]

[a]Dynamics and Vibration Unit, ENTEG, Faculty of Science and Engineering, University of Groningen, Groningen, The Netherlands; [b]Industrial Systems Engineering and Design Group, Dept. Mech. Aer. Eng. (DIMEAS), Politecnico di Torino, Torino, Italy

ABSTRACT

This study develops a Quad-Finger structure as a multimodal vibration energy harvester using macro fiber composites (MFCs). Comprising piezoelectric fibers in a polymer matrix, MFCs offer enhanced mechanical robustness and address the brittleness of traditional piezoceramics, making them ideal for vibration energy harvesting applications. The proposed Quad-Finger structure is consisting of a primary plate, four smart beams embedded with MFC patches, and proof masses. To assess the harvester's performance in real applications, a read-out circuit is integrated to measure the electrical outputs. A finite element (FE) model is developed using COMSOL Multiphysics® 6.0 to simulate the harvester's performance. The read-out circuit is also simulated in LTspice, allowing the FE results to be validated and the circuit to be optimized. Following the simulations, a prototype of the harvester is fabricated, and experimental tests are conducted to verify the simulation results and demonstrate practical performance. The FE model enables extensive numerical analysis, showing that the device effectively harvests vibrational energy from its first four modes within a 10 Hz bandwidth, highlighting its potential for broadband vibration energy harvesting. Notably, MFCs prove to be significantly more efficient for energy harvesting compared to traditional piezoceramics. Furthermore, power output analysis suggests that the harvester operates optimally when a tunable load resistance is employed.

ARTICLE HISTORY
Received 8 January 2025
Accepted 6 February 2025

KEYWORDS
Vibration energy harvesting; piezoelectric harvester; smart structures; multimodal systems; structural mechatronics

1. Introduction

Piezoelectric harvesters offer promising prospects for harnessing energy from ambient vibration. This harvested energy is of significant importance in energizing low-power electronics, such as wireless sensor nodes (WSNs), portable devices, and medical implants. In recent years, there has been a growing interest in vibration-based energy harvesting [1–8], due to the issues with conventional power sources (i.e. chemical batteries). The objective in this research area is to provide power to small electronics by capturing the vibrational energy available in their environment. If successful, this approach can potentially reduce the reliance on chemical batteries, decrease maintenance costs related to their frequent replacement, and mitigate the environmental impact of battery disposal.

Piezoelectric materials, such as piezoceramics (PZTs), known for their high electromechanical coupling properties, large power densities and ease of application have become a focal point for vibration energy harvesting applications. However, the traditional PZTs are brittle and highly sensitive to tensile strain, making them unsuitable for applications involving large deformations or cyclic loads. To overcome such issues, macro fiber composite (MFC) materials were developed by NASA Langley Research Center in 1999 [9]. MFCs are consisting of rectangular piezo ceramic rods sandwiched between layers of adhesive, electrodes, and polyimide film. The electrodes are attached to the film in an interdigitated pattern which transfers the applied voltage directly to and from the ribbon-shaped rods. This assembly enables in-plane poling, actuation, and sensing in a sealed, durable, and ready-to-use package. Such materials are available globally through Smart Material Corporation [9], and come in various types: P1, P2, and P3. The P1-type MFCs utilize the electromechanical coupling effect between electric field and mechanical strain in the same direction (as is described by coefficient d_{33} [10]), and function as highly sensitive strain sensors. The P2- and P3-type MFCs operate based on the coupling effect between two orthogonal directions, namely 3 for electric filed and 1 for mechanical strain (as described by coefficient d_{31} [10]), and are primarily used for piezoelectric energy harvesting (PEH) and as strain sensors. The P3-type MFC, which consists of wider fibers, exhibits behavior similar to an orthotropic, monolithic piezoceramic plate when compared to the P2-type. This causes the P3-type MFC to be less flexible than the P2- or P1-type MFCs.

In dynamic systems, the primary source of mechanical energy typically arises from ambient vibration within the system or its surroundings. Piezoelectric-based energy harvesters, particularly those configured as cantilever beams, predominantly operate in the transverse mode (d_{31} mode)

CONTACT M. Askari m.askari@rug.nl

and utilize one or more layers of piezoelectric material (i.e., unimorph or bimorph configurations) [11]. In such configurations, the bending of the beam results in a normal stress along the axial direction on the piezoelectric material, which leads to generation of electrical charge. In the field of piezoelectric vibration energy harvesting, the literature indicate that the energy efficiency is dependent on the electromechanical coupling effect, damping effect, excitation frequency and electrical load [5,12–17]. Environmental vibration sources typically have varying frequencies and magnitudes over time, posing a challenge in generating sufficient power from dynamic excitation. Research efforts are underway to address those challenges and enhance energy harvesting efficiency. Given these considerations, systems incorporating multiple vibration modes have been proposed as potential designs for broadband vibration energy harvesting [18–20]. Roundy et al. [21] introduced this concept for the first time, incorporating multiple proof masses to achieve a wider bandwidth. Building upon this concept, Yang et al. [22] developed an electromagnetic energy harvesting beam with multiple magnets serving as proof masses and voltage-inducing components. Tadesse et al. [23] presented a cantilever harvester integrated with hybrid energy harvesting schemes, each efficient for a specific mode. Based on similar principles, many more research works have been presented in the recent years to address broadband energy harvesting [24–27]. However, in such proposed designs, either the high-order vibration modes are often significantly separated from the fundamental mode, or the power efficiency remains low. Moreover, the efficiency of piezoelectric energy harvesting is determined by how the charge extracted from the piezoelectric generator is managed. An interface circuit or a circuit for rectifying and conditioning the electrical charge [28] is typically required to convert the alternating current from the piezoelectric material into direct current suitable for powering the load. Designing the read-out circuit necessitates careful selection of its electrical components as well as an examination of the linked electromechanical dynamics.

In this study, an MFC-based Quad-Finger multimodal harvester is designed, fabricated, and experimentally validated. The proposed device addresses the critical challenge of matching the resonance frequencies of the harvester with those of real-world applications, which is an essential design consideration for resonance-based energy harvesters. Additionally, through the integration of a suitable read-out circuit, the harvester effectively resolves the issue of voltage cancelation, which commonly occurs in piezoelectric harvesters utilizing multiple generators.

The structure of this paper has been organised as follows: *Section 2* outlines the design of the harvester, providing a detailed description of its layout and the electrical circuits used for measuring the outputs. *Section 3* discusses the finite element (FE) modeling conducted in COMSOL software, while *Section 4* describes the experimental setup used to validate the FE model. *Section 5* presents a comprehensive comparison of the numerical and experimental results, alongside an in-depth analysis of the harvester's performance. Lastly, *Section 6* concludes the work by summarizing the key findings and suggesting directions for future research.

2. The proposed energy harvester

2.1. Harvester design and constitutive equations

The schematic design of the Quad-Finger harvester is shown in Figure 1(a). The idea of incorporating four beams in the proposed design was initially inspired by the structure of the human hand, excluding the thumb. The structure consists of a substrate layer, MFC patches (d_{31}-mode), and proof masses. The substrate layer is divided into two parts: a plate, with length a, width b, and thickness t, as well as four cantilever beams, with identical width w and thickness t, that are connected to the free side of the plate (see Figure 1(b)). The lengths of the beams are not identical as they span from L_1 to L_4 in Figure 1(b). Also, the parameters d and s denote the gap between the beams and the distance between the closest edge of the plate and *beam* 1 and *beam* 4, respectively. It is worth noting that the composition of the substrate layer is continuous and can be simply fabricated from a rectangular sheet in practice. Also, the MFC layers have active and inactive parts, where the inactive part is composed of only Polyimide film ($L_i \times W_i \times t_i$), and the active part is a symmetric composite of five laminated layers ($L_a \times W_a \times t_a$). The active part consists of rectangular piezoceramic rods (made of PZT-5A) sandwiched between layers of adhesive, electrodes, and polyimide film (see Figure 2). The electrodes are attached to the film in an interdigitated pattern which transfers the applied voltage directly to and from the ribbon-shaped rods. Last components in the proposed harvester are the proof masses that are identical, being long L_m, wide w, and thick h_m.

As shown in Figure 1(a), three edges of the substrate layer are clamped, and the entire device is intended to experience base excitation along the z-direction. This excitation induces mechanical strain within the MFC layers (in particular, within the piezoceramic rods), which is then converted into electric charge through the electromechanical coupling provided by piezoelectricity. It is commonly known that piezoelectric materials generate electric charges when subjected to mechanical deformation, and they produce strain when an electric field is applied to them. These two phenomena are called the *direct* and *converse* effects of piezoelectricity. The direct piezoelectric effect forms the foundation of piezoelectric energy harvesters (PEHs). However, both direct and converse piezoelectric effects are described by the following constitutive equations, respectively:

$$\{\varepsilon\} = [S^E]\{\sigma\} - [d]^T\{E\} \tag{1a}$$

$$\{D\} = [d]\{\sigma\} - [\in^\sigma]\{E\} \tag{1b}$$

Equations (1a) and (1b) establish a connection between the mechanical domain (stress σ and strain ε) and the electric domain (electric field E and displacement field D). In Eq. (1), $[S]$, $[d]$, and $[\in]$ correspond to the compliance

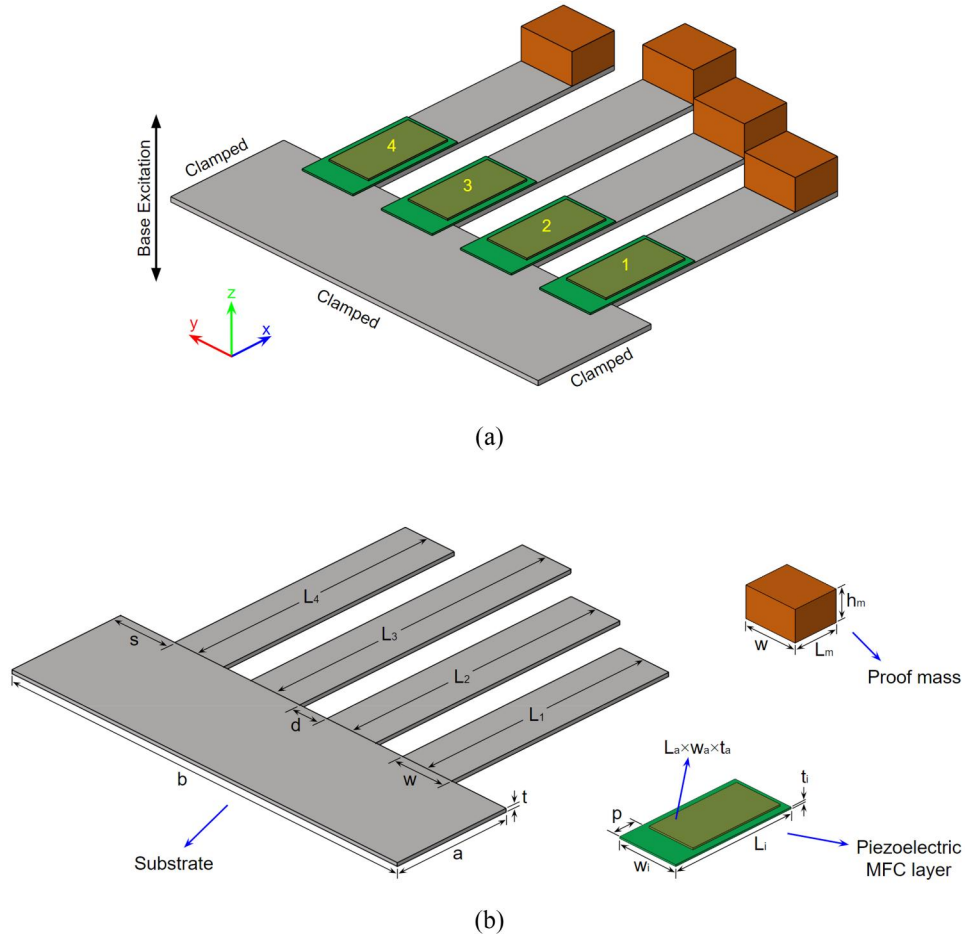

Figure 1. Schematic representation of the proposed piezoelectric energy harvester.

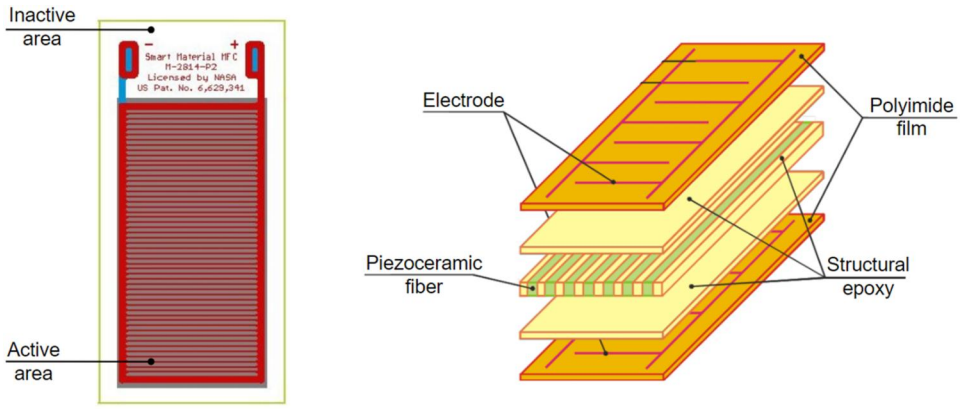

Figure 2. MFC microstructure [9].

matrix, electromechanical coefficients matrix, and the dielectric permittivity matrix, respectively, and they can be expressed in the following forms for piezoelectric materials polarized in z-direction (i.e. d_{31}-mode):

$$[S^E] = \begin{bmatrix} S_{11}^E & S_{12}^E & S_{13}^E & 0 & 0 & 0 \\ S_{21}^E & S_{22}^E & S_{23}^E & 0 & 0 & 0 \\ S_{31}^E & S_{32}^E & S_{33}^E & 0 & 0 & 0 \\ 0 & 0 & 0 & S_{44}^E & 0 & 0 \\ 0 & 0 & 0 & 0 & S_{55}^E & 0 \\ 0 & 0 & 0 & 0 & 0 & S_{66}^E \end{bmatrix} \quad (2a)$$

$$[d] = \begin{bmatrix} 0 & 0 & 0 & 0 & d_{15} & 0 \\ 0 & 0 & 0 & d_{24} & 0 & 0 \\ d_{31} & d_{32} & d_{33} & 0 & 0 & 0 \end{bmatrix} \quad (2b)$$

$$[\in^\sigma] = \begin{bmatrix} \in_{11}^\sigma & 0 & 0 \\ 0 & \in_{22}^\sigma & 0 \\ 0 & 0 & \in_{33}^\sigma \end{bmatrix} \quad (2c)$$

To fully describe the MFC materials in COMSOL software, the components of the three-dimensional elastic compliance (S_{ij}^E), piezoelectric (d_{ij}), and relative permittivity ($\in_{ij}^\sigma$) matrices are required, while such materials data are not

directly available from the data sheet provided by their manufacturer (i.e. Smart Material Corporation). According to the supplier's data sheet [9] and Refs. [29,30], the available electrical and mechanical properties of MFCs are given in Table 1.

However, the three-dimensional compliance matrix of the MFC can be constructed by converting the linear elastic engineering constants provided by the manufacturer [9] (given in Table 1) into Eq. (3). This equation was derived from the standard stress-strain relations for orthotropic materials, as presented in [32]. The resulting compliance matrix follows the standard form for a transversely isotropic material, with crystalline symmetry perpendicular to the poling direction.

$$[S^E] = \begin{bmatrix} \frac{1}{E_1} & \frac{-\nu_{12}}{E_1} & \frac{-\nu_{12}}{E_1} & 0 & 0 & 0 \\ \frac{-\nu_{12}}{E_1} & \frac{1}{E_2} & \frac{-\nu_{21}}{E_2} & 0 & 0 & 0 \\ \frac{-\nu_{12}}{E_1} & \frac{-\nu_{21}}{E_2} & \frac{1}{E_2} & 0 & 0 & 0 \\ 0 & 0 & 0 & \frac{2(1+\nu_{21})}{E_2} & 0 & 0 \\ 0 & 0 & 0 & 0 & \frac{1}{G_{12}} & 0 \\ 0 & 0 & 0 & 0 & 0 & \frac{1}{G_{12}} \end{bmatrix} \quad (3)$$

where E_i is the Young's modulus along axis i, G_{ij} is the shear modulus in direction j on the plane whose normal is in direction i, and ν_{ij} is the Poisson's ratio that corresponds to a contraction in direction j when an extension is applied in direction i. The final S_{ij}^E used to define the compliance matrix of the MFC patches is:

$$[S^E] = \begin{bmatrix} 3.30 & -1.02 & -1.02 & 0 & 0 & 0 \\ -1.02 & 6.31 & -1.01 & 0 & 0 & 0 \\ -1.02 & -1.01 & 6.31 & 0 & 0 & 0 \\ 0 & 0 & 0 & 14.63 & 0 & 0 \\ 0 & 0 & 0 & 0 & 18.13 & 0 \\ 0 & 0 & 0 & 0 & 0 & 18.13 \end{bmatrix} \times 10^{-11}\ \mathrm{m^2N^{-1}} \quad (4)$$

Additionally, due to the symmetric property of PZTs, the $d_{31} = d_{32}$ and $d_{24} = d_{15} = 0$ [29]. Therefore, matrix $[d]$ can also be reduced to the following matrix:

$$[d] = \begin{bmatrix} 0 & 0 & 0 & 0 & 0 & 0 \\ 0 & 0 & 0 & 0 & 0 & 0 \\ d_{31} & d_{31} & d_{33} & 0 & 0 & 0 \end{bmatrix} \quad (5)$$

The matrix $[d]$ does not include shear piezoelectric coefficients (e.g. d_{15}). While typical piezoelectric ceramics such as PZT-5A and PZT-5H have nonzero d_{15} values, in many composite materials, $|d_{15}|$ is significantly smaller than $|d_{3j}|$ [29]. Moreover, since the electric field is always oriented along the poling direction, shear piezoelectric coefficients are not expected to contribute.

The relative permittivity of the active layer is also required to accurately characterize the electromechanical coupling within the MFC layer. This property is important for relating charge, capacitance, and voltage for the MFC materials, and it influences the magnitude of the induced electric field under mechanical stress. In this study, the relative permittivity values are taken from Ref. [31] and are given in Table 1. Ref. [31] validates the accuracy of this simulation approach for MFCs against the experimental results for a cantilever harvester. Thus, with the properties specified in the $[S^E]$, $[d]$, and $[\in^\sigma]$ tensor forms, MFCs can be adequately modeled in COMSOL software.

Table 1. Mechanical and electrical properties of MFC patches.

	Material property	Unit	Value
Active part [9,29,31]	Tensile modulus in rod direction, E_1	GPa	30.336
	Tensile modulus in electrode direction, E_2	GPa	15.857
	Shear modulus, G_{12}	GPa	5.515
	Poisson's ratio, v_{12}	1	0.31
	Poisson's ratio, v_{21}	1	0.16
	Volume density, ρ	kg/m^3	5440
	$d_{31} = d_{32}$	pC/N	−170
	d_{33}	pC/N	400
	$\in_{11}^{\sigma}$	1	712
	$\in_{22}^{\sigma}$	1	1.7
	$\in_{33}^{\sigma}$	1	737
Inactive part (Polyimide film) [30]	Young's modulus, E	GPa	1.85
	Volume density, ρ	kg/m^3	1140
	Poisson's ratio, v	1	0.34

2.2. Power management circuit

The harvester device is intended to be located on a vibrating host structure, where the dynamic strain induced in the MFC layers leads to an alternating voltage output across their electrodes. An alternating voltage output is obtained owing to, for instance, a harmonic base motion applied to the structure. In the mechanics research on piezoelectric energy harvesting as well as in the experimental research aimed at assessing the device performance for AC power generation, it is common practice to consider a simple resistor as electrical load [33–36] (see Figure 3). In the case of a harvester with multiple piezoelectric generators (such as in bimorph configurations or the design proposed in this study), the piezoelectric electrodes can be wired, for instance, in parallel or series configurations. In Figure 3, V represents the AC voltage generated by the piezoelectric layer, and R_L indicates the electrical load. Integrating such electrical circuit with the harvester helps optimize the mechanical design of the device and understand the effect of various parameters, such as the electrical load, on the electromechanical response of the harvester.

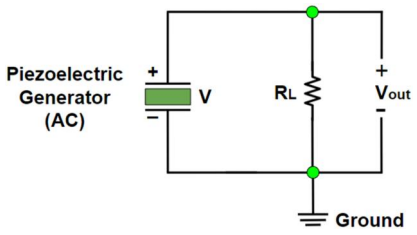

Figure 3. Typical configuration of a piezo harvester with a simple resistor.

However, although a piezoelectric component that vibrates produces an AC voltage, the electrochemical battery necessitates a DC voltage [37]. To optimize energy management and load delivery, the harvester requires a power management circuit (also known as read-out circuit) that rectifies, stores, and conditions the energy produced. This ensures electrical compatibility with the load being supplied. Figure 4 shows an energy harvesting read-out circuit for a single piezoelectric generators, which is consisting of:

- *Diode bridge (D_1 to D_4)*: blocks the return of charges from the circuit to the piezoelectric material while rectifying the current. This allows for the storage of both positive and negative charges.
- *Capacitance (C)*: records the energy transferred in individual events; the intermediate storage capacity protects the piezoelectric material by preventing charge build-up.
- *DC/DC converter*: simulates the optimal load impedance and adjusts the output voltage to prevent the battery discharge or saturation.
- *Battery*: stores the charge and powers the electronic equipment to which it is attached.

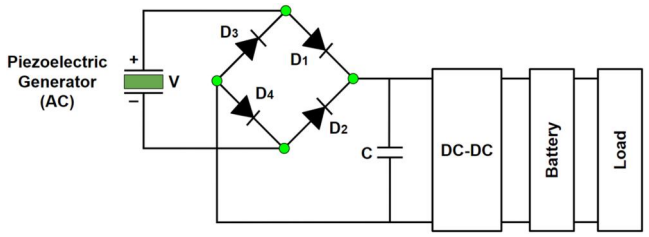

Figure 4. Power management module for a single generator.

- *Load*: refers to the electrical device or component that consumes or utilizes the harvested energy.

Considering the aforementioned read-out circuit, different electrical configurations are herein designed for wiring the multiple piezoelectric generators in the proposed multimodal harvester. These configurations, (i.e. series and parallel circuits) are schematically illustrated in Figure 5. The DC-DC and battery modules are omitted from the following read-out circuit models, as the primary focus is on effectively designing the AC-DC rectifier, which helps prevent voltage cancelation. In systems with multiple piezoelectric generators, voltage cancelation can occur due to phase differences in the voltage outputs. Each generator produces a voltage in response to the mechanical vibrations it experiences. However, when generators experience vibrations out of sync (e.g. one reaching a peak while another hits a trough), the resulting voltages can have opposite signs (i.e. positive and negative) at certain moments, which may lead to partial or complete cancelation if combined without rectification. To address this issue in the proposed harvester, each generator has been paired with a rectification stage (using a diode bridge), which converts the AC output to DC form, enabling combination of generators without interference.

The rectifier diode bridges in the circuits shown in Figure 5 are independent of the piezoelectric sources, which are arranged in two distinct configurations: series (Figure 5(a)) and parallel (Figure 5(b)). In the series configuration, the total voltage is the sum of the voltages generated by each piezoelectric element, allowing for higher voltage outputs. However, this arrangement can present a problem if one of the piezoelectric sources fails, as the entire system's

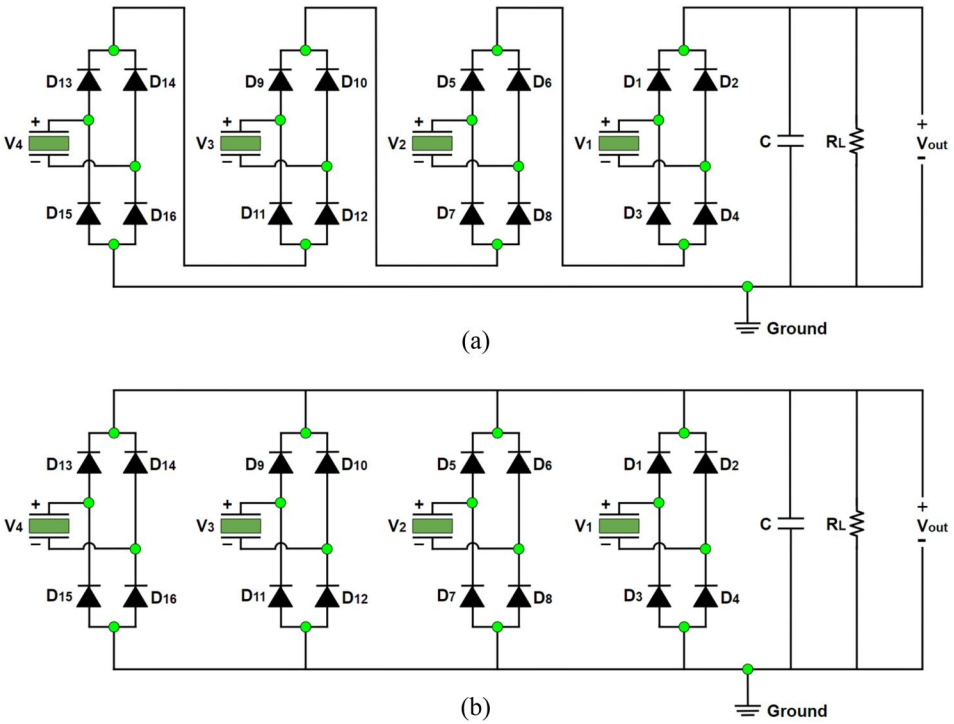

Figure 5. The read-out circuit for the proposed harvester with multiple generators in (a) series, (b) parallel configuration.

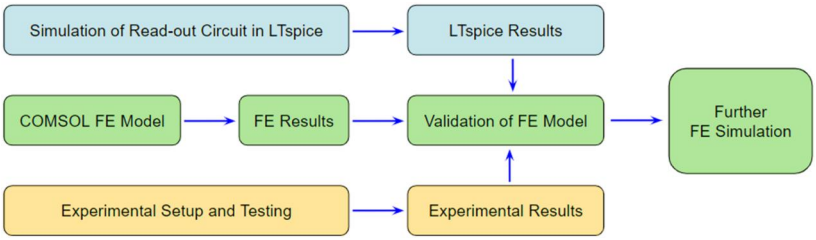

Figure 6. Block diagram of the methodology employed in the present work.

voltage output may be compromised, with each element affecting the total voltage generated. Furthermore, charge cancelation remains an issue in the series configuration, as the internal current (I_{0i}) can vary significantly between different sources. If I_{0i} is less than the load current (I_L), a source will be charged in reverse (with output current $I_i = I_{0i} - I_L < 0$). By converse, the parallel configuration mitigates some of these problems. In this arrangement, the circuit assures read-out and charge transferring even when one generator fails, and it can generate a larger current, which is advantageous for accelerating the charging process of the storage capacity [38].

It should be noted that concerning energy harvesters with multiple generators, when the sources are in phase and can be treated as a single source, it is straightforward to connect them in series or parallel before a shared rectifier, as done with a single source in a standard circuit [39,40]. However, this configuration is not feasible if the sources have different frequencies and are out of phase. In such cases, when the frequency of an excitation wave deviates from the generators' resonance frequencies, the phase difference between the produced voltages is minimal. However, this difference significantly widens when the excitation frequency approaches the resonant frequencies [41].

3. Finite element (FE) modelling

The proposed harvester design is initially simulated in COMSOL software, which allows for precise coupling of multiple physics and accurate definition of their associated boundary conditions. The resulting FE model is then validated against experimental results and simulations conducted in LTspice XVII software. To achieve this, a numerical modal analysis is performed using the FE model, with the results first validated by those of experimental modal analysis using shaker testing (this is further explained in subsection 5.1). Subsequently, the read-out circuits shown in Figure 5 are simulated in both COMSOL and LTspice, and a comparative study of the outcomes of both simulations is conducted. After validation of the FE model, additional simulations are performed in COMSOL to evaluate the performance of the harvester. A block diagram representing the current methodology is presented in Figure 6.

Utilizing the geometrical data of the scavenger, given in Table 2, the FE model of the harvester is initially constructed in COMSOL software. The harvester layout is first sketched within the 3D environment of COMSOL, where

Table 2. Geometrical data of the proposed harvester.

Component	Geometrical parameter	Value (mm)
Substrate	b	130
	a	40
	t	1
	w	18
	d	10
	s	14
	L_1	80
	L_2	90
	L_3	100
	L_4	85
MFC layers (2814-P2)	L_i	37
	w_i	18
	t_i	0.15
	L_a	28
	w_a	7
	t_a	0.3
	p	7.5
Proof masses	L_m	15
	h_m	10

different modules and physics can be integrated into the FE model based on the study requirements. At this stage, different materials are also assigned to various domains of the harvester. In particular, the substrate is made of Aluminum (with Young's modulus of 70 GPa, mass density of 2700 kg/(m^3), and Poisson's ratio of 0.3), piezoelectric layers are made of MFC materials, and proof masses are made of Stainless Steel (with Young's modulus of 193 GPa, mass density of 8000 kg/(m^3), and Poisson's ratio of 0.3).

In the design of vibration energy harvesters, performing modal analysis is always helpful to compute the natural frequencies and mode shapes of the device. This can be achieved in COMSOL software by conducting an eigenfrequency study. For that, the proposed harvester is first meshed using tetrahedral elements (with fine element size), after which an eigenfrequency study is performed. The outcome of this investigation will be presented in Section 5, where the numerical results are discussed in detail.

Once the eigenfrequencies of the system are known, frequency-domain studies can be conducted within specific frequency bands, which include the resonance frequencies, to extract the frequency response of the scavenger. It is important to note that the frequency-domain study conducts FE analysis of the system for each given frequency, which is then utilized to extract comprehensive results presented in frequency response plots. To construct the model, the *Solid Mechanics* module is integrated with the *Electrostatics* and *Electrical Circuit* modules. The Solid Mechanics module

facilitates the set-up of material damping, constraints, and loading conditions for the structure. Additionally, the Electrostatics and Electrical Circuit modules enable the configuration of electrical boundary conditions for piezoelectric materials, such as Terminals and Ground. These electrical parameters are then linked to the Electrical Circuit module, where the circuits described in Subsection 2.2 are composed.

The material properties and geometrical parameters of the harvester are considered based on the data provided in Tables 1 and 2, respectively. Also, the harmonic base excitation is simulated as a body force in COMSOL, which is applied to the entire structure.

After presenting an overview of the structure's performance in the frequency domain, the transient behavior of the coupled system will be investigated through the time domain analysis. Prior to integrating the read-out circuit depicted in Figure 5, it is necessary to conduct a circuit analysis in LTspice XVII to understand the dynamics and refine the settings for circuit energy efficiency. The electronic component libraries and graphical interface in LTspice facilitate faster analysis of iterations involving various piezoelectric input generators and their impact on the performance of the power storage capacitor. However, the utilization of COMSOL Multiphysics is essential in this study because, unlike LTspice, which employs a simplified representation of the electromechanical system, COMSOL enables complete coupling of both mechanical and electrical physics, leading to a more realistic simulation.

Upon designing the read-out circuit, the LTspice Netlist is exported and integrated into COMSOL's Electrical Circuit module. To finalize the implementation of the time domain analysis and closely replicate the behavior of the actual device, the pulse shape must be defined with a time-varying law to excite the model base. The voltage curves generated at the piezoelectric layer terminals will be exported from COMSOL and imported into LTspice to verify the accuracy of the time domain analysis.

4. Fabricated harvester and experimental setup

A prototype of the proposed harvester has been fabricated at the Technical Support Department of the Faculty of Science and Engineering at the University of Groningen, and is shown in Figure 7. The harvester device is consisting of of a housing part (for clamping), the multi-beam substrate, piezoelectric patches, and proof masses. As mentioned earlier, the piezoelectric patches are made of MFC materials, which are commercially available by Smart Material Corporation [9]. In particular, MFC-2814-P2 patches are used here as piezoelectric generators and are manually attached to the substrate layer using epoxy adhesive (Loctite® E-120HP). The MFC patches are electrically connected in parallel configuration using 24AWG Hookup wires (CNC Tech-3239-24-1-0500), as recommended by their manufacturer [9]. The wires were soldered to the electrodes of the MFC patches to ensure optimal conductivity when measuring the electrical outputs.

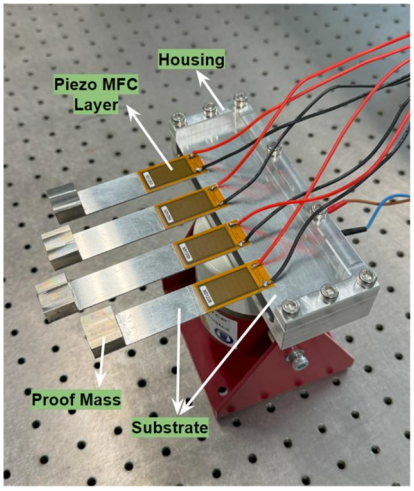

Figure 7. The harvester prototype placed on the electrodynamic shaker device.

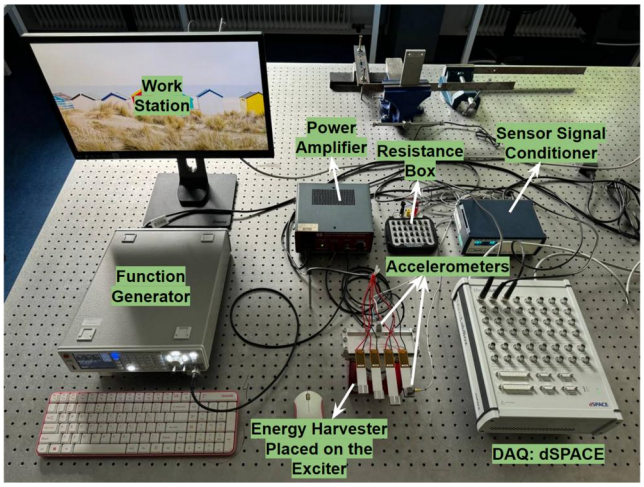

Figure 8. Experimental setup provided for energy harvesting measurements.

In order to measure the electrical outputs to base excitation, an experimental setup, shown in Figure 8, was prepared. The setup includes a data acquisition system (dSPACE MicroLabBox), an electrodynamic shaker (Data Physics GW-V4), a power amplifier (Data Physics - PA30E), a function generator (Rohde & Schwarz - HMF2525 25 MHz), two accelerometers (Bruel & Kjaer – 4507), and a resistance box (VOLTCRAFT R-BOX 02). A diagram illustrating this setup is also provided in Figure 9.

To measure the voltage generated by the harvester, a signal is first generated by the function generator, then amplified and supplied to the shaker, which is eventually applied to the structure as base excitation. Two accelerometers are placed on the clamping part and on a proof mass to measure the vibration response of the system. One of the accelerometers measures the base acceleration, while the other measures the acceleration response on the proof masses. The setup enables various vibration tests on the harvesting structure.

5. Model validation and discussion

In this section, the FE model is validated, and comprehensive numerical and experimental results are presented and

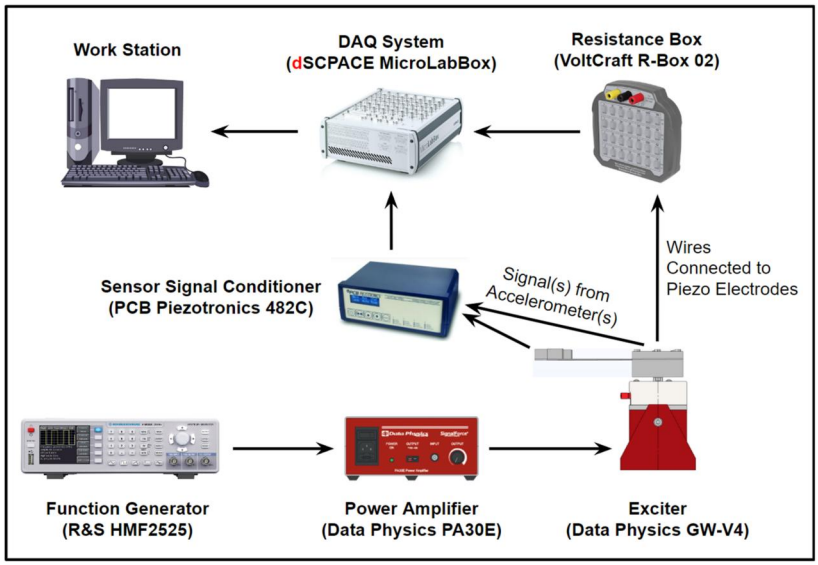

Figure 9. Schematic diagram of the experimental setup.

thoroughly discussed. First, a static analysis was conducted in COMSOL to explain the placement of MFC patches in the Quad-Finger structure (see Figure 1(a)). For this study, the harvester was considered without the MFC layers, and a total load of 20 N was applied to the free ends of the beams in the thickness direction (i.e. 5 N per beam). The goal was to plot the bending normal strain distribution within the substrate layer as the structure experienced bending deformation. The results, shown in Figure 10, depict the mechanical strain distribution in the x-direction. It is evident that the strain is concentrated along the length of the beams, with the maximum values near the clamps where they connect to the substrate plate. Consequently, for optimal electrical charge generation, MFC patches should be placed in regions with the highest strain. This placement remains effective for vibration energy harvesting, provided the focus is on the first four modes of the Quad-Finger harvester (see Figure 11), where only the fundamental bending mode of each beam is engaged. Thus, the MFC patches (specifically, their active areas) are bonded to the substrate layer in regions experiencing maximum bending deformation during base excitation.

However, before the FE model can be used to explore the electromechanical response of the scavenger, it must be validated in terms of both dynamic and electrical responses. Subsection 5.1 presents a validation study, comparing the numerical results from the FE model with experimental measurements. Following this, the effects of mechanical and electrical parameters, as well as the system's dynamic characteristics, on the harvester's behavior are demonstrated and discussed in the subsequent subsections.

5.1. Validation study

The initial investigation involves performing a modal analysis using the FE COMSOL model and the experimental setup. Figure 11 presents the results of the eigenfrequency study conducted in COMSOL, revealing the first four resonance frequencies of the scavenger as 17.9, 22.2, 25.4, and 27.9 Hz, respectively. To validate these findings, an experimental vibration test was conducted using shaker excitation. A sweep-sine signal with frequencies ranging from 12 to 32 Hz was applied to the harvester base, and the voltage response was measured in the time domain (see Figure 12). To monitor the base excitation, an accelerometer was mounted on the harvester housing to measure acceleration along the z-axis. Figure 12 shows the magnitude of the frequency response function from the test. The frequency values corresponding to the peaks are 18.1, 22.4, 25.9, and 28.4 Hz for the first, second, third, and fourth vibration modes, respectively. These results are also summarized in Table 3, alongside their counterparts from the COMSOL model. As shown in Table 3, there is excellent agreement between the numerical and experimental results, demonstrating the accuracy of the FE model. However, the slight differences between the results may be attributed to the adhesive layers between the MFC patches and the substrate, which are not included in the FE model. Additionally, the fabricated proof masses differ slightly in weight, whereas they are completely identical in the FE model. There may also be a minor positioning error in the experimental setup, as the proof masses at the free ends were placed manually.

In another validation study, the open-circuit voltage output of the harvester was measured as a function of excitation frequency for a harmonic base excitation of 0.1 g (g is the acceleration of gravity and equals 9.81 m/s^2). The effect of structural damping has been simulated by defining a an isotropic loss factor of 5% in the FE model [42,43]. The voltage FRF computed from the FE model is shown in Figure 13. For comparison, harmonic base excitation with an amplitude of 0.1 g was applied to the harvester at each of its resonance frequencies, and the corresponding generated voltage and power outputs were measured at open circuit mode. These results are presented in Table 4 alongside those calculated from the FE simulations. Table 4 shows that the electrical outputs predicted by the FE simulations align with

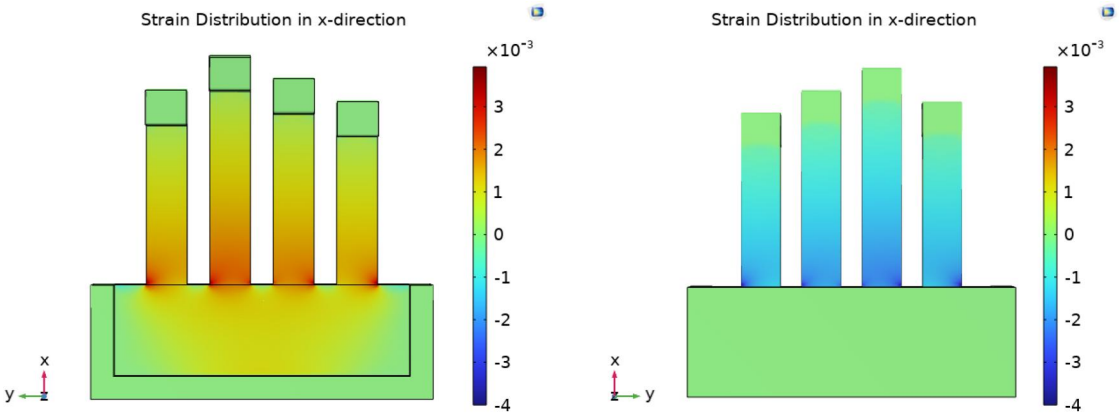

Figure 10. Distribution of axial strain under bending load.

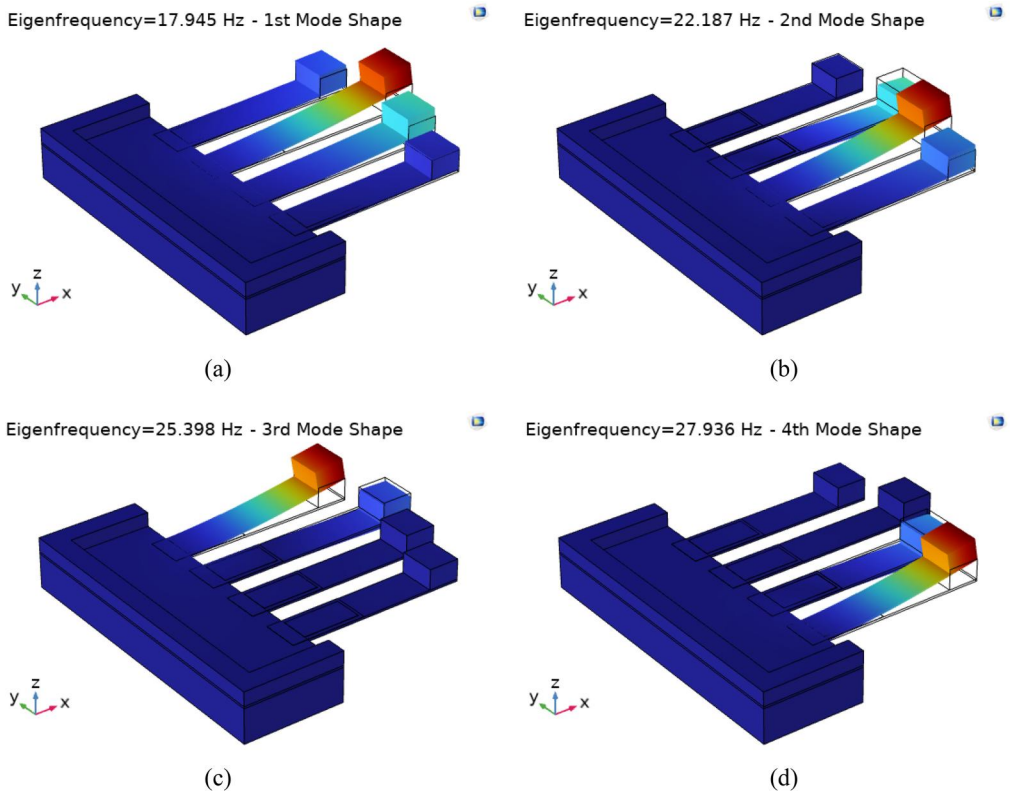

Figure 11. The first four vibration mode shapes of the proposed harvester.

the experimental measurements, though the FE model tends to underestimate the voltage and power outputs at the harvester's resonance frequencies. These discrepancies are likely due to the simplified simulation of the electromechanical characterization of the MFC layers. While micromechanical modeling of MFCs could yield more accurate results, its complexity makes it too computationally expensive for integration within a larger macro-scale structural model. However, this study, again, confirms the accuracy of the FE model which can now be used as a reference for obtaining new results and investigating the effects of various parameters on the mechanical and electrical response of the scavenger.

In the following subsections, the effects of various parameters on the mechanical and electrical response of the harvester are analyzed. It is important to note that the results presented in subsections 5.2 are based on the harvester equipped with MFC generators connected in parallel, with a purely resistive electrical load (see Figure 3). In subsection 5.3, the read-out circuits previously shown in Figure 4 are separately integrated with the harvester, and the corresponding results are presented and discussed.

5.2. Harvester integrated with an electrical resistor

As demonstrated in the previous subsection, the harvester exhibits four bending vibration modes, which are the first four modes of the system and are of interest for vibration-to-electricity conversion in this study. Higher vibration modes (i.e. 5th, 6th, …) are less effective for vibration

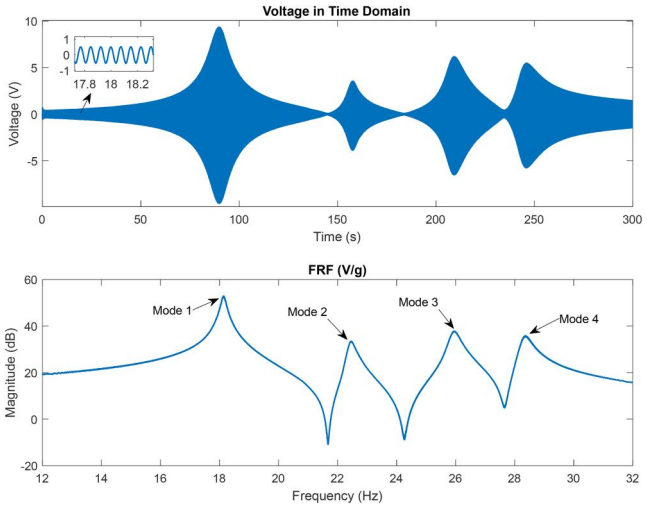

Figure 12. Experimental time-domain and frequency-domain results from the sweep sine vibration testing.

Table 3. FE simulations and experimental results for the harvester's resonance frequencies (Hz).

Vibration mode	FE simulation	Experiment	Difference
1st Mode	17.9	18.1	1.1%
2nd Mode	22.2	22.4	0.9%
3rd Mode	25.4	25.9	1.7%
4th Mode	27.9	28.4	1.8%

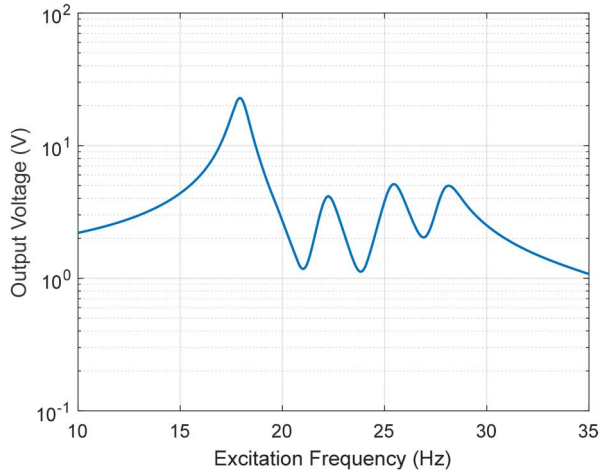

Figure 13. FE simulation results for the output voltage of the harvester at open circuit mode.

Table 4. Comparison of OC voltage and power amplitude computed from the FE simulations and experimental results.

	Voltage (V)		Power (μW)	
Vibration mode	FE simulation	Experiment	FE simulation	Experiment
1st Mode	22.8	≅ 23.0	5.20	≅ 5.29
2nd Mode	4.2	≅ 4.5	0.18	≅ 0.20
3rd Mode	5.1	≅ 6.8	0.26	≅ 0.46
4th Mode	5.0	≅ 5.3	0.25	≅ 0.28

energy harvesting due to the presence of more strain nodes (i.e. points where the dynamic strain distribution changes sign in the direction of beam length), as well as lower motion amplitude. For instance, covering the strain nodes with continuous electrodes leads to significant voltage cancellation. To avoid this issue, precise alignment of the piezoelectric patches with the deformation pattern, as well as complex design considerations for electrodes and wiring, is required [44]. Even with careful alignment and design, the power efficiency from higher vibration modes is typically low, and these modes are difficult to excite in practical vibration energy harvesting applications. Therefore, this study focuses on harvesting energy using the first four vibration modes of the proposed scavenger, which involve only the fundamental bending mode of each beam (see Figure 11). When the excitation frequency aligns with one of those modes (i.e. resonance frequency(s) of the scavenger), resonance occurs, leading to a significant amount of strain within the MFC layers. This mechanical strain is converted into electrical charge through the electromechanical coupling of the piezoelectric materials embedded in the microstructure of the MFCs.

Figure 14 shows the voltage frequency response of the harvester under base harmonic excitation, with amplitudes ranging from 0.1 g to 0.5 g, applied across a frequency range of 10 to 35 Hz. The harvester is here assumed to operate in open-circuit mode (null current), which is modeled in the FE simulation by setting a very high value for the electrical load [45]. As shown in Figure 14, four voltage peaks appear in the frequency response curves when the excitation frequency matches the harvester's resonance frequencies. This notable feature of multimodal harvesters potentially addresses the frequency matching issue commonly associated with single degree-of-freedom (single-DOF) harvesters. With the proposed harvester, electric power can be generated over a frequency band and without relying solely on a single frequency. As expected, applying base excitation with higher acceleration amplitudes results in greater voltage output, as increased mechanical strain is induced within the MFC layers. Since the proposed harvester is a linear system, the output voltage increases linearly as the base excitation rises. Additionally, it can be observed from Figure 14 that as the excitation level increases, the harvester generates a higher voltage over a broader frequency band. Specifically, when a base acceleration of 0.5 g is applied, the scavenger produces a voltage of at least 10 V across nearly the entire excitation frequency range from 10 to 31 Hz. This demonstrates that the device can effectively harvest energy even when not operating at resonance. Also, a maximum stress of approximately 120 MPa is observed in the Aluminum component when the harvester is subjected to a base acceleration of 0.5 g at its first resonance, while lower stress values are recorded for the other modes. Although higher voltage output can be achieved with increased input excitation (i.e. greater than 0.5 g), it is associated with higher stress levels, increasing the likelihood of device failure in practice. Therefore, higher input excitations are not considered and are excluded from this study, and the device is not intended for use in environments where large amplitude vibrations exist.

As observed thus far, the harvester achieves maximum voltage output at the excitation frequencies of 17.9, 22.2, 25.4, and 27.9 Hz, which corresponds to the first four vibration modes of the harvester. Figure 15 illustrates the effect

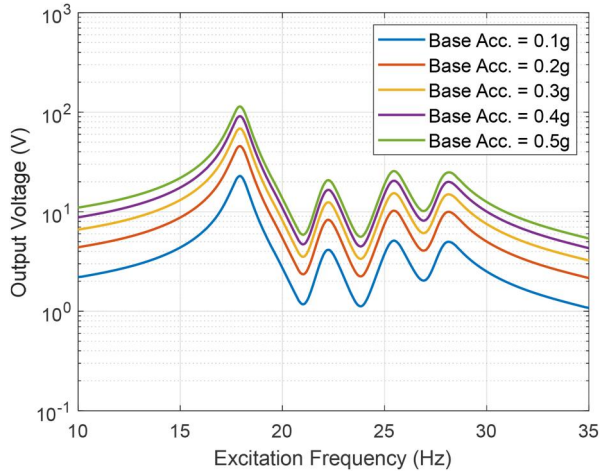

Figure 14. Open-circuit voltage frequency response for different excitation amplitudes ($R_L = 10\,G\Omega$).

of electrical load R_L on the harvester's voltage and power response when the device is excited at the mentioned frequencies. From the figure, it can be observed that the voltage and power collection efficiency is the highest in the first mode, followed by mode 3, mode 4, and mode 2, for the device being excited at the same base acceleration level. This is because the first mode represents the dominant bending mode, which induces larger oscillations compared to the higher modes. While the first four modes correspond to the first bending mode of each cantilever, it appears that in the first mode, the cantilevers oscillate in phase. In contrast, in the higher modes, the cantilevers oscillate out of phase, with one cantilever moving upward while the other moves downward. This phase difference causes voltage cancelation, resulting in reduced power generation efficiency in the higher modes. Additionally, regarding the effect of the electrical load, Figure 15(a) demonstrates that the output voltage increases with a higher electrical load integrated into the harvesting system. It is known that small values of R_L simulate the short-circuit mode, while large values of R_L represent the device operating in the open-circuit mode. Given this, the device produces higher voltage output in open-circuit mode, as expected. However, a different trend is observed in Figure 15(b) concerning the power generated by the harvester as a function of the electrical load. Notably, there is an optimized value of R_L at which the maximum output power is achieved. This optimized value of R_L appears to be dependent on the excitation frequency, with values of 305, 255, 225, and 210 kΩ for the first mode and subsequent modes, respectively, based on Figure 15(b). Therefore, if a constant electrical load is consistently employed, the harvester will not operate at maximum efficiency (in terms of power generation) across all excitation frequencies.

So far, the FE simulation results have indicated that the voltage response of the harvester increases as the load resistance increases (see Figure 15(a)). However, this investigation was initially limited to the excitation frequencies corresponding to the resonance frequencies of the harvester. To extend this analysis, the effect of load resistance is studied

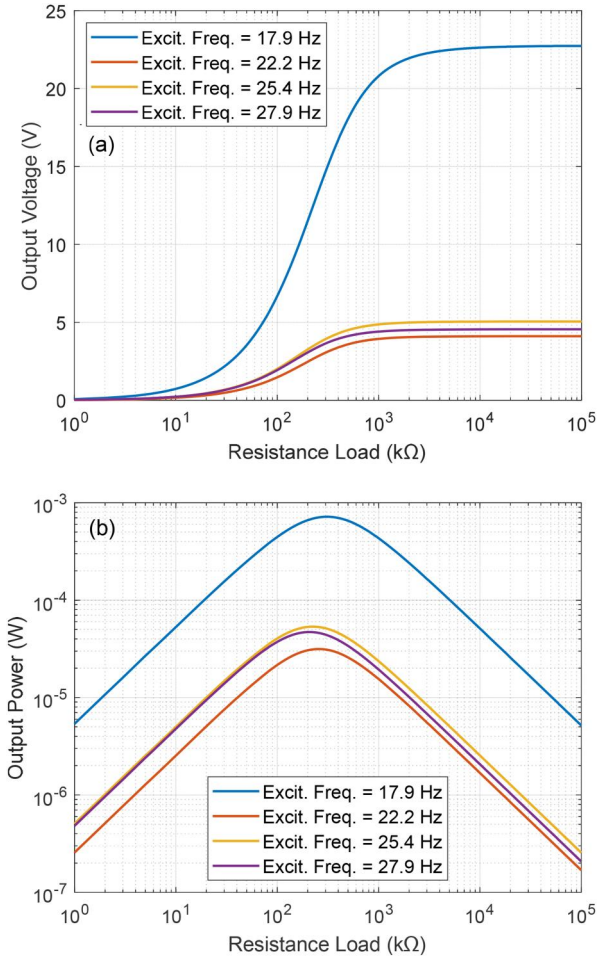

Figure 15. Voltage and power outputs versus the electrical load (base Acc. = 0.1 g).

experimentally over a broader frequency range of 12 to 32 Hz. The corresponding results are presented in Figure 16, which illustrates the harvester voltage response in both time and frequency domains, for different values of load resistance, namely 10^2,10^3,10^4, 10^5, 10^6, and 10^7 Ω. For the experimental testing, the harvester was excited at its base using a sweep-sine signal over the frequency range of 12 to 32 Hz. Note that the amplitude of the base acceleration was varying in this test as it is a function of displacement amplitude and the excitation frequency. However, the voltage response is measured with the four piezo patches connected in a parallel configuration. These experimental results align with the findings from FE simulations, confirming the same conclusion regarding the effect of electrical load on the harvester's voltage response.

To provide a deeper insight into the effect of electrical load, the output power is plotted in Figure 17 against R_L for base excitation at resonance frequencies but with different excitation levels of 0.2, 0.3, 0.4 and 0.5 g. One can observe from Figure 17 that, again, at each excitation frequency (which is, in fact, not limited to resonance frequencies), there exists an optimal value of R_L that maximizes power generation. Also, the figures reveal that the optimized values of R_L (at various excitation frequencies) are almost independent of the level of input excitation for the proposed linear scavenger.

However, in practice, the proposed scavenger can always operate at its optimal condition (i.e. consistently generating maximum power) by using a variable electrical load [46] that adjusts according to the base excitation frequency.

Depending on the dynamic characteristics of ambient vibration in a target application and the available space for implementing an energy harvester, different types of optimization studies can be conducted to design the harvester in the most effective way. For example, the geometry of the harvester can be optimized to achieve the highest possible electrical outputs for the same input mechanical energy (or base excitation) into the system. However, a complete optimization study requires knowledge of the specific target application, which is not the focus of the present study. Nonetheless, as an example, to illustrate how the geometry of the proposed harvester affects electrical outputs, a parametric study is conducted, showing the impact of the plate width in the substrate part (denoted as '*a*' in Figure 1(b)) on the output voltage. Assuming the OC electrical condition, the voltage frequency response of the harvester as a function of the excitation frequency is plotted in Figure 18 for different values of *a*, ranging from 10 mm to 70 mm. It is seen from the figure that increasing the width of the plate leads to a harvester with lower resonance frequencies associated with the first four modes. However, the trends for the output voltage peaks corresponding to various modes are different. Specifically, as the value of *a* increases, the output voltage peak corresponding to the fundamental mode rises, while a descending trend is observed for the higher modes. The values of output voltage corresponding to the peaks are

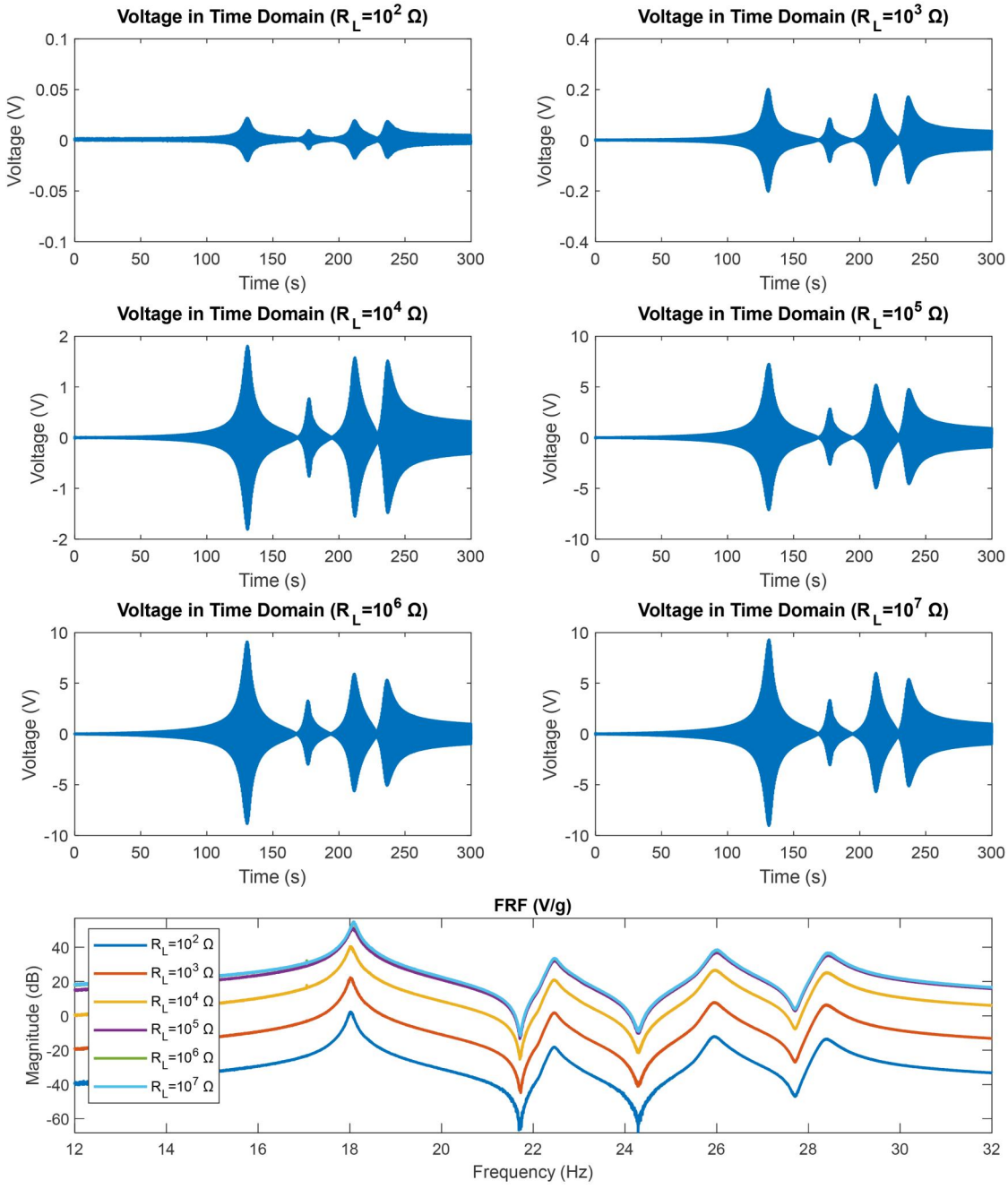

Figure 16. Voltage response of the harvester in both time and frequency domains.

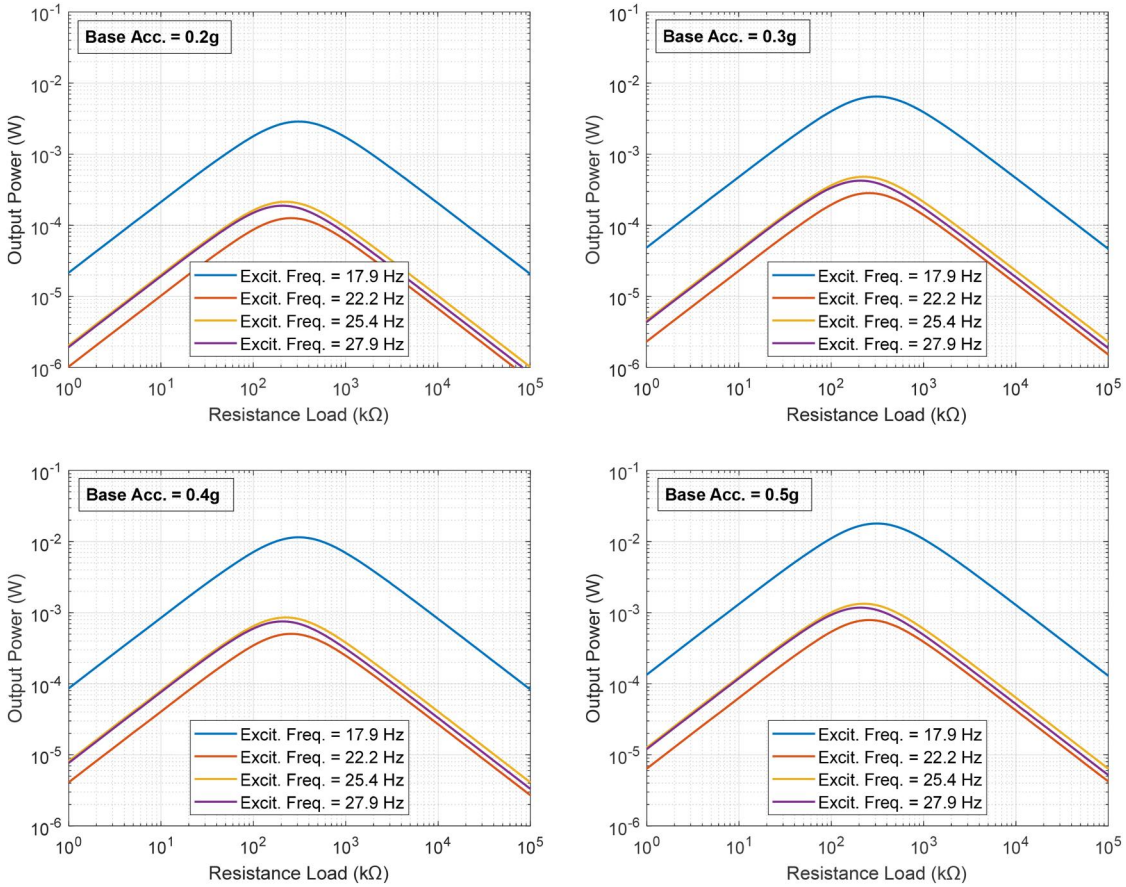

Figure 17. Power output versus the electrical load for various excitation amplitudes.

extracted from Figure 18 and listed in Table 5 along with the associated resonance frequencies for harvesters with different values of *a*. It is concluded that increasing the value of *a* decreases the overall open-circuit voltage that can be generated by the harvester. As anticipated, changing this parameter significantly influences both the mechanical and electrical responses of the scavenger.

The harvester prototype allows for adjusting the width of the plate substrate (i.e. *a*) to two different values: 10 mm and 40 mm. For both configurations, a harmonic base excitation over the frequency range of 12 to 32 Hz (i.e. a sweep sine signal) was applied to the harvester, and the resulting open-circuit voltage response is presented in Figure 19. The experimental results, consistent with the FE model results presented in Figure 18, confirm that reducing the substrate width increases the resonance frequencies of all modes. This reduction leads to a decrease in the peak voltage of mode 1 but an increase in the peak voltage of modes 2, 3, and 4.

Instead of MFC generators, PZT-5A and PZT-5H generators of the same size (i.e. $28 \times 14 \times 3$ mm) were also used separately for energy conversion, and the FE model was updated accordingly. The materials properties of PZT-5A and PZT-5H are given in Table A1 in the Appendix [47]. The results for a base excitation level of 0.5 g were obtained for three cases: *Case* 1: harvester with four MFC generators; *Case* 2: harvester with four PZT-5A generators; and *Case* 3: harvester with four PZT-5H generators. The results are presented in Figure 20. The figure clearly shows that using

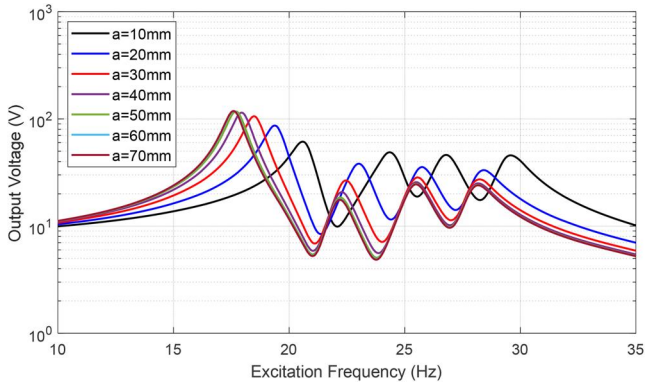

Figure 18. Open-circuit voltage frequency response of the harvester for different values of *a* (base Acc. = 0.5 g).

MFC generators results in significant voltage enhancement across the entire frequency band, and the harvester exhibits lower resonance frequencies compared to a harvester integrated with piezoceramic generators. Specifically, with MFC generators, the voltage output from the first vibration mode is approximately 58% and 97% higher than when using PZT-5A and PZT-5H, respectively. These voltage enhancements are around 77% and 120% for the second mode, 70% and 111% for the third mode, and 72% and 113% for the fourth mode. Additionally, PZT-5A patches consistently demonstrate better energy harvesting performance compared to PZT-5H.

Table 5. Numerical results extracted from Figure 18.

	Open-circuit voltage (V)				
a (mm)	1st mode	2nd mode	3rd mode	4th mode	Total
10	61.4 (at 20.6 Hz)	48.9 (at 24.3 Hz)	46.1 (at 26.8 Hz)	45.8 (at 29.6 Hz)	202.2
20	86.7 (at 19.4 Hz)	38.2 (at 23.0 Hz)	35.6 (at 25.7 Hz)	33.2 (at 28.4 Hz)	193.7
30	105.8 (at 18.5 Hz)	26.6 (at 22.5 Hz)	28.5 (at 25.6 Hz)	27.3 (at 28.2 Hz)	188.2
40	114.4 (at 18.0 Hz)	20.8 (at 22.3 Hz)	25.7 (at 25.5 Hz)	25.0 (at 28.2 Hz)	185.9
50	117.5 (at 17.7 Hz)	18.5 (at 22.2 Hz)	24.8 (at 25.5 Hz)	24.2 (at 28.2 Hz)	185.0
60	118.4 (at 17.6 Hz)	17.8 (at 22.2 Hz)	24.5 (at 25.5 Hz)	24.0 (at 28.2 Hz)	184.7
70	118.6 (at 17.6 Hz)	17.6 (at 22.2 Hz)	24.5 (at 25.5 Hz)	24.0 (at 28.2 Hz)	184.7

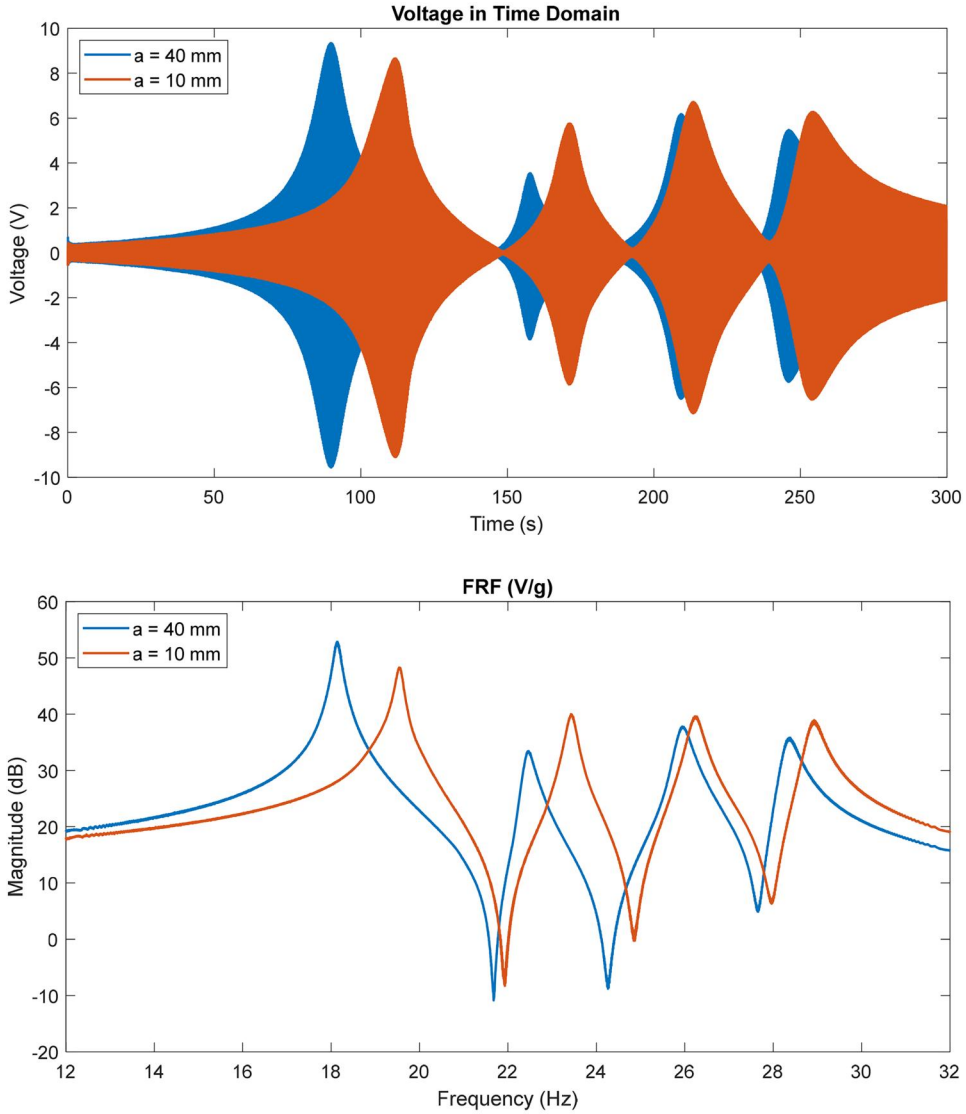

Figure 19. Open-circuit voltage output of the harvester for different values of *a* (experimental results).

The substrate material in a piezoelectric vibration energy harvesting system is crucial as it provides mechanical support for the piezoelectric layers and affects the overall mechanical characteristics of the device such as flexibility, durability, and resonance frequency. Here, instead of Aluminum, the substrate is assumed to be made of FR4 (with $E = 26\,\text{GPa}$, $\rho = 1900\,\text{kg/m}^3$, and $\nu = 0.17$ [48]), a composite material with high mechanical strength (tensile yield strength of 340 MPa). With an FR4 substrate (along with MFC generators and Steel proof masses), the voltage

frequency response of the harvester to base excitation across the 5 to 25 Hz frequency band was calculated and is presented in Figure 21. Different values of '*a*' were also considered. Figure 21 shows that both the mechanical and electrical responses are significantly influenced by replacing the Aluminum substrate with FR4. As seen, for the harvester with the narrowest substrate width (i.e. $a = 10$ mm), the resonance frequencies are shifted to lower values of 13.7, 16.2, 17.9, and 19.8 Hz for modes 1 to 4, respectively. Compared to the results in Figure 18 (that are for Aluminum substrate), the harvester with FR4 substrate generates much higher voltage peaks at resonance for all vibration modes.

As the final investigation in this subsection, the following comparison highlights the differences in electromechanical response between the proposed Quad-Finger harvester and a conventional cantilever harvester, which represents the fundamental design for vibration energy harvesting. Figure 22 compares the peak values of voltage frequency responses of the two designs under a base excitation of 0.5 g for the first four bending modes. It is important to note that other vibration modes, aside from bending, are not considered here, as the d_{31}-type piezoelectric patches are specifically used for vibration energy harvesting from bending modes. The cantilever harvester used for comparison shares the same geometry as the first beam in the Quad-Finger harvester (see Figure 1). The substrate, piezoelectric patch, and proof mass are composed of the same materials (Aluminum, MFC 2814-P2, and Stainless Steel, respectively). As observed from Figure 22, the resonance frequencies of the cantilever harvester are significantly spaced apart for its bending modes, making it challenging to effectively harvest energy from the higher bending modes when it comes to practical applications. This difficulty arises from the presence of additional strain nodes in higher modes and the increasing complexity of the mode shapes. Additionally, these higher modes are often heavily damped, diminishing their efficiency for energy harvesting. Moreover, it is practically impossible to find an application where vibrational energy is consistently available over a frequency band that covers both the fundamental mode and the higher modes of a cantilever harvester. As a result, harvesting energy from the higher modes of a cantilever is neither practical nor efficient, as significantly lower voltage levels (compared to the fundamental mode) are generated. In contrast, the proposed Quad-Finger harvester exhibits its first four bending-type modes with closely spaced frequencies, as shown in Table 5 (see also in Figure 11). These four vibration modes involve only the fundamental bending mode of each beam, which is a key advantage of the proposed harvester. Importantly, the harvester is capable of generating voltage from its higher modes (i.e. 2nd, 3rd and 4th modes), with values comparable to that of the fundamental mode. The fact that the first four resonances fall within a 10 Hz frequency band is particularly advantageous for practical applications, where the frequency

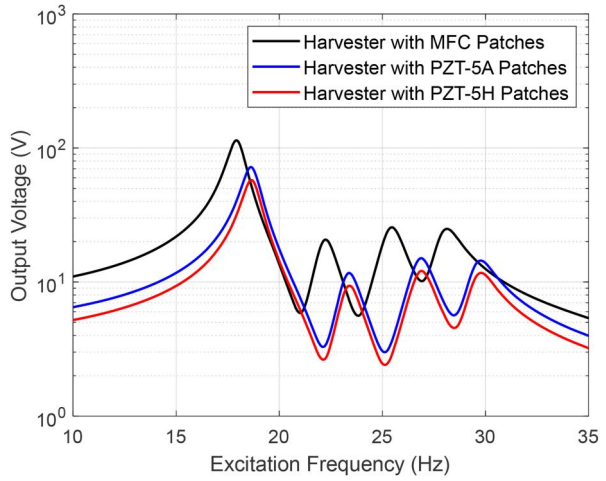

Figure 20. Open-circuit voltage frequency response of the harvester with different piezoelectric materials (base Acc. = 0.5 g).

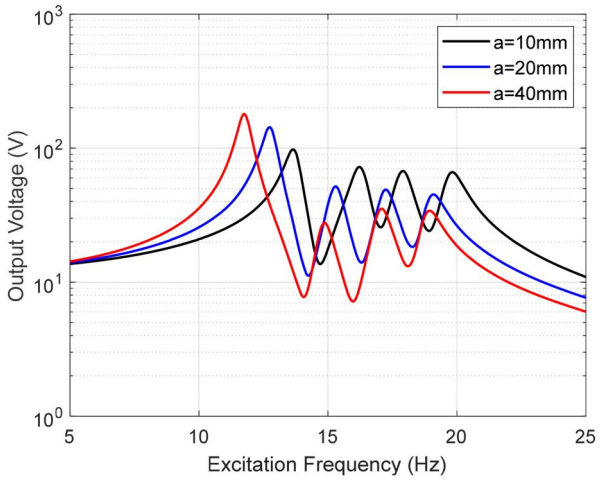

Figure 21. Open-circuit voltage frequency response of the harvester with substrate made of FR4 (base Acc. = 0.5 g).

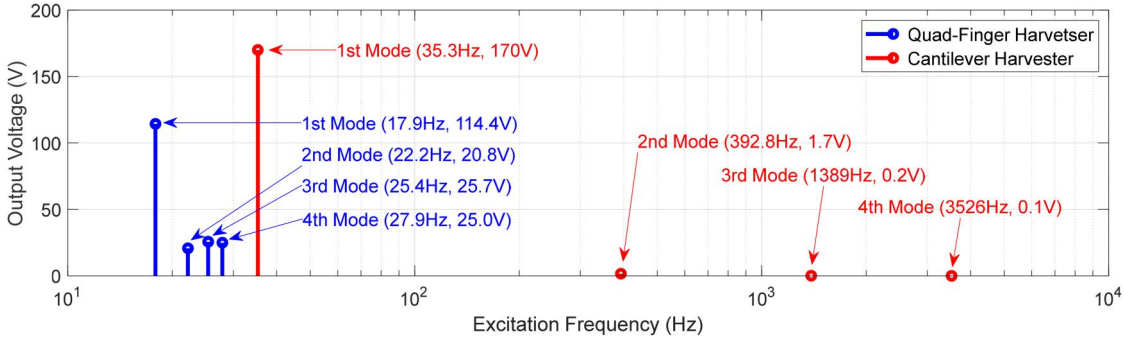

Figure 22. Comparison of the electromechanical responses of the Quad-Finger harvester and a cantilever harvester.

of ambient vibrations often fluctuates. This feature allows for effective vibration energy harvesting even when deviations from the first mode occur, as the higher modes can still be activated, leading to significant voltage generation. The results in the previous figures also confirm that the Quad-Finger harvester can harvest energy under base excitation, even out of resonance, as long as the excitation falls within the 10 Hz bandwidth that includes its first four resonances.

5.3. Harvester integrated with power management circuit

After analyzing the harvester's performance in the frequency domain, it is important to simulate real-world operating conditions. Most electronic devices require a stable power source, as the charge must be rectified and accumulated before being supplied to the device. To address this, the proposed harvester was integrated with the readout circuits depicted in Figure 5, and the model was accordingly adjusted. On the other hand, the system's dynamics and electronic components were simulated and analyzed in LTspice software (see Figure A1 in the Appendix), to optimize energy extraction from the piezoelectric generators. The circuit includes a 5 μF storage capacitor (indicated by C_1), a 90 kΩ resistor (indicated by R_1), Schottky 1N5817 diodes (selected to minimize voltage drops [49]), and piezoelectric generators, represented as alternating voltage sources V_1 to V_4. Note that the 90 kΩ resistor was identified as the electrical load that place the harvester in open-circuit mode. This value was determined through computations performed in LTspice. The aforementioned electrical components were also implemented in the read-out circuit of the COMSOL model.

As a validation study, a comparison between the results of the COMSOL model and LTspice was performed. A time-domain study in COMSOL was carried out in which a harmonic base excitation of 0.5 g was applied to the harvester at excitation frequency of 25 Hz. The voltage generated at the terminals of the four piezoelectric generators was extracted for both parallel and series configurations and imported into the LTspice model using PWL files (see Figure A1). These measurements were used as inputs for the LTspice model, and the voltage accumulated on the capacitor C_1 was then measured in both models, with the results plotted in Figure 23. It is observed that, for both parallel and series configurations, the voltage curves overlap entirely, demonstrating an excellent match between the results of the COMSOL and LTspice models. This validation confirms the accuracy of the read-out circuit simulation in the FE COMSOL model. Additionally, Figure 23 shows that the parallel configuration achieves a higher voltage in the capacitor compared to the series configuration. This is because, in a parallel setup, each cantilever independently contributes to charging the capacitor, maintaining the same voltage while summing the currents. In contrast, the series configuration relies on the combined voltages from each cantilever, but the current flow is limited by the sequential connection of components, leading to reduced energy storage efficiency. This comparison highlights the superior energy efficiency of the parallel configuration, offering valuable insights into selecting the optimal architecture for energy harvesting devices.

After validating the read-out circuit simulation in COMSOL, the finite element (FE) model was employed to assess the time-domain response of the Quad-Finger harvester when excited at its fundamental resonance frequency (i.e. the first mode). Considering parallel electrical configuration for the read-out circuit, the device was harmonically excited with a base amplitude of 0.5 g at a frequency of 17.9 Hz. The resulting voltage and charge outputs on the capacitor C_1 are shown in Figure 24. It is observed that the harvester generates an output voltage of 45 V and 225 μC charge after a period of 1 s. This output is expectedly lower than the voltage produced by the harvester when integrated with a simple resistor and without additional electrical components such as diodes. The reduced voltage output is attributed to the electrical damping or voltage drop caused by the other components in the read-out circuit. The presence of these components, particularly the diodes, introduces voltage losses, reducing the energy delivered to the storage capacitor.

The voltage behavior across the capacitor over time illustrates the charge accumulation process from the four piezoelectric generators. The rate at which the voltage increases reflects the efficiency of the piezoelectric patches and the rectifier circuit components in transferring charge. Achieving 45 V in 1 s signifies a well-optimized system, where the component dimensions and the integration of the piezoelectric characteristics of the cantilevers with the storage mechanism work efficiently. This level of charge generation (i.e. 225 μC) demonstrates the piezoelectric system's capacity to supply significant energy within a short time, making it promising for powering low-consumption devices. The effectiveness of charge accumulation and voltage conversion depends on both the mechanical behavior of the harvester and the rectification circuit, which converts the alternating charge into direct current.

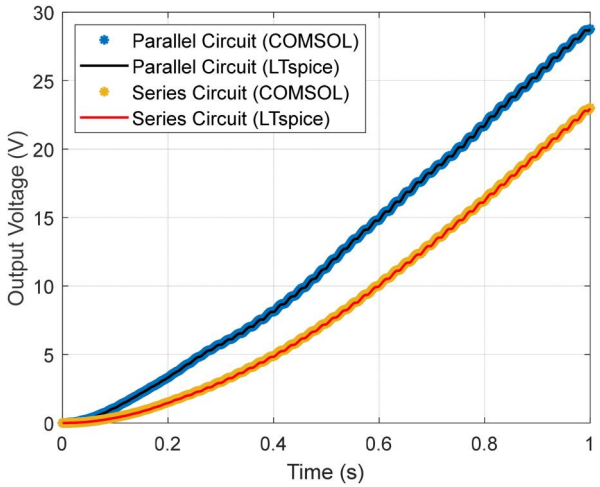

Figure 23. Comparison of the results calculated from the FE and LTspice models for the harvester integrated with the read-out circuit (base Acc. = 0.5 g).

5.4. A Demonstration example of the proposed harvester

The proposed harvester was tested in the lab to demonstrate its practical potential. An LED board module (with three LEDs commercially available from Smart Material Corporation [9]) was directly connected to the piezoelectric generators (while they are parallelly wired). The LEDs can be illuminated one by one depending on the frequency and the level of acceleration induced by shaking the harvester. For this purpose, the device was excited at its base at resonance frequencies, and its performance near the first to fourth vibration modes was monitored. The results, shown in Figure 25, were captured in photos. Notably, the harvester successfully powered one LED when excited at its vibration modes. As expected, higher excitation amplitudes would result in more LEDs being powered. The demonstration example highlights the practicality of the proposed energy harvester. Additionally, the harvester is well-suited for complex working environments with wide-band, time-varying, and random characteristics, owing to its multimodal energy harvesting capability.

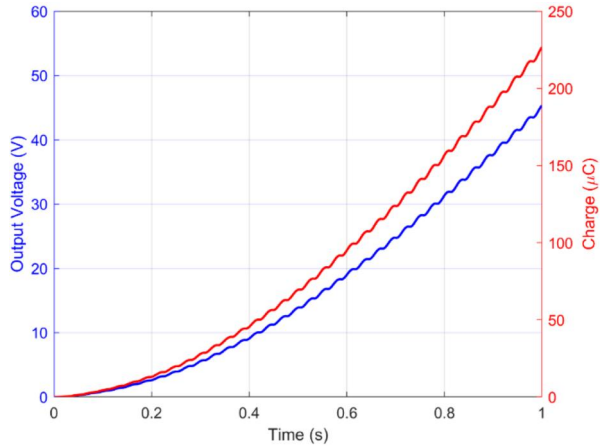

Figure 24. Voltage and charge time response for the harvester with read-out circuit excited at its first vibration mode (base Acc. = 0.5 g).

6. Conclusion

In this study, a novel Quad-Finger multimodal structure was proposed and experimentally tested for broadband vibration energy harvesting. An FE model was developed in COMSOL to estimate the device's output voltage and power under harmonic base excitation. The FE model was validated against experimental results and simulations performed in LTspice, after which it was used to explore the harvester's behavior. The key findings of the study are summarized as follows:

- An FE energy harvesting model was successfully developed in COMSOL Multiphysics to simulate the electromechanical response of MFCs.
- The harvester exhibited its first four vibration modes of bending type, with resonance frequencies of 18.1, 22.4, 25.9, and 28.4 Hz. As a result, the multimodal harvester could potentially generate electrical energy when excited within a frequency range including the scavenger's resonance frequencies.
- The effect of load resistance on output power was investigated, revealing that the output power is highly dependent on the resistance. The device can produce more power across a broad frequency range by incorporating a tunable load resistance.
- The proposed harvester demonstrated significantly better performance with MFC layers compared to typical piezoceramics such as PZT-5A and PZT-5H. Thus, the use of MFCs is highly recommended for energy harvesting applications.
- The results of this study provide guidelines for designing broadband vibration harvesters using MFCs, with the goal of maximizing energy harvesting performance.

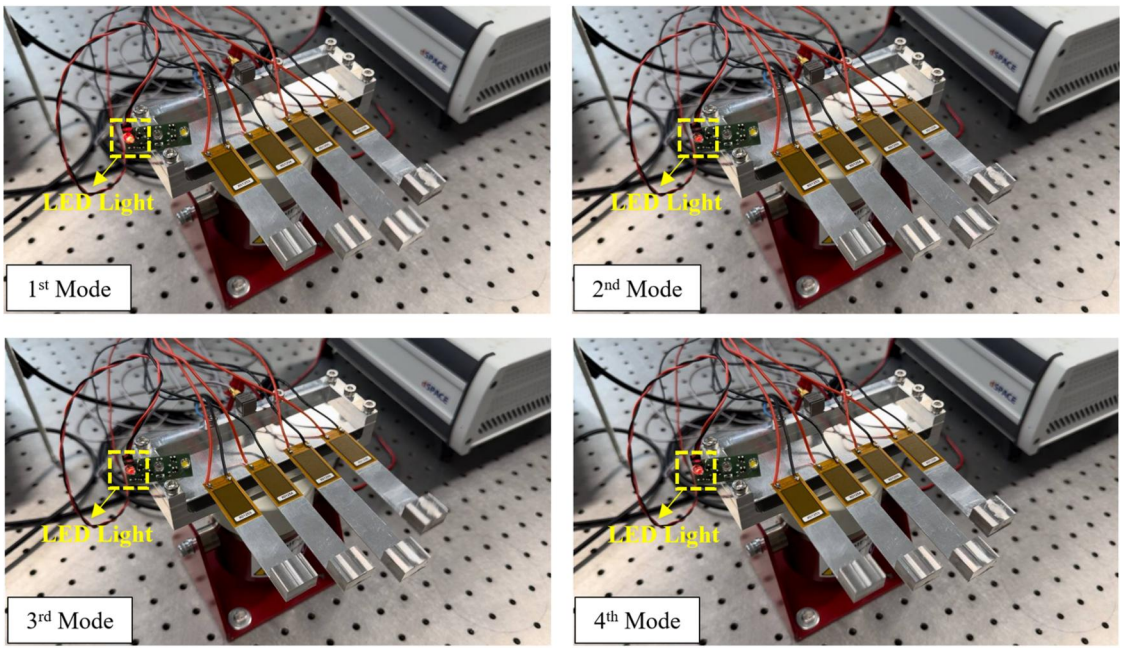

Figure 25. An example of practical application of the proposed harvester.

- When the read-out circuit was integrated, the harvester generated an output voltage of 45 V in open-circuit mode within 1 s. Using diode bridges in a parallel configuration, rather than in series, allows for higher voltage output, faster capacitor charging, and improved stability and safety. This setup protects the circuit from overloads while ensuring more uniform charge distribution across the system.

The system demonstrates notable efficiency in converting mechanical energy into electrical energy. Achieving the optimal balance between piezoelectric coupling and the dynamics of the read-out circuit enhances the overall energy harvesting performance by maximizing charge generation and transfer to the storage circuit.

The Quad-Finger harvester may have various practical applications, particularly in wireless sensor networks (WSNs), where power is limited or inaccessible. By harvesting ambient vibrations, it can provide a sustainable energy source, reducing reliance on traditional batteries and associated maintenance costs. Additionally, the system holds potential for safety-critical applications, including medical implantable devices for pressure monitoring, sensors to stent transmitters, and pacemakers, ensuring a constant and reliable power supply.

Future works will focus on optimization studies to enhance the harvester's electrical output for specific target applications. Additionally, refinements to the experimental setup are planned, including the integration of a complete read-out circuit and other essential electronic components, with the goal of developing a fully autonomous sensor node powered by the energy harvester. This device is aimed to eventually be tested in real-world applications to evaluate its performance under practical conditions.

Acknowledgements

The authors would like to acknowledge the support of Technical Support Department (FTD) at the University of Groningen for their collaboration in the fabrication of the harvester device.

Declaration of interest

The authors declare that there are no potential conflicts of interest regarding the research, authorship, or publication of this article.

Funding

This research was co-funded by FSE REACT-EU Azione IV.5 "Dottorati su tematiche Green" of the Italian Ministry for University and Research Activity, under decree D.M. 1061/2021, and by the Research Group ISED, at Dept. Mechanical and Aerospace Engineering, Politecnico di Torino.

ORCID

M. Askari http://orcid.org/0000-0001-5135-0850
M. Ghandchi Tehrani http://orcid.org/0000-0002-0824-4937
E. Brusa http://orcid.org/0000-0001-7478-0650
A. Carrera http://orcid.org/0000-0001-8631-9650
C. Delprete http://orcid.org/0000-0002-0220-4707

References

[1] Z. Yang, S. Zhou, J. Zu, and D. Inman, High-performance piezoelectric energy harvesters and their applications, Joule., vol. 2, no. 4, pp. 642–697, 2018. DOI: 10.1016/j.joule.2018.03.011.
[2] M. Safaei, H.A. Sodano, and S.R. Anton, A review of energy harvesting using piezoelectric materials: state-of-the-art a decade later (2008–2018), Smart Mater. Struct., vol. 28, no. 11, pp. 113001, 2019. DOI: 10.1088/1361-665X/ab36e4.
[3] P. Kurt, B. Narayan, J.I. Roscow, and S. Orhan, Improving piezoelectric energy harvesting performance through mechanical stiffness matching, Mech. Adv. Mater. Struct., vol. 31, no. 28, pp. 10721–10734, 2024. DOI: 10.1080/15376494.2023.2295383.
[4] S.S. Raju, M. Umapathy, and G. Uma, Design and analysis of high output piezoelectric energy harvester using non uniform beam, Mech. Adv. Mater. Struct., vol. 27, no. 3, pp. 218–227, 2020. DOI: 10.1080/15376494.2018.1472341.
[5] D.S. Ibrahim, Y. Feng, X. Shen, U. Sharif, and A.A. Umar, On geometrical configurations of vibration-driven piezoelectric energy harvesters for optimum energy transduction: a critical review, Mech. Adv. Mater. Struct., vol. 30, no. 7, pp. 1340–1356, 2023. DOI: 10.1080/15376494.2022.2031357.
[6] M.T. Mhiri, M. Chouchane, M. Guerich, and W. Larbi, Modeling and analysis of a macro-fiber piezoelectric bimorph energy harvester operating in d33-mode using Timoshenko theory, Mech. Adv. Mater. Struct., vol. 31, no. 30, pp. 13021–13035, 2024. DOI: 10.1080/15376494.2024.2331597.
[7] X. Huang, X. Hua, and Z. Chen, Exploiting a novel magnetoelastic tunable bi-stable energy converter for vibration energy mitigation, Nonlinear Dyn., vol. 113, no. 3, pp. 2017–2043, 2025. DOI: 10.1007/s11071-024-10337-z.
[8] X. Huang, Exploiting multi-stiffness combination inspired absorbers for simultaneous energy harvesting and vibration mitigation, Appl. Energy., vol. 364, pp. 123124, 2024. DOI: 10.1016/j.apenergy.2024.123124.
[9] Smart Material Corporation, n.d. Available: https://www.smart-material.com/. Accessed: Sep. 6, 2024.
[10] IEEE Standard on Piezoelectricity, ANSI/IEEE Std 176-1987, approved September 7, 1987.
[11] G. Gatti, M.J. Brennan, M.G. Tehrani, and D.J. Thompson, Harvesting energy from the vibration of a passing train using a single-degree-of-freedom oscillator, Mech. Syst. Signal Process., vol. 66-67, pp. 785–792, 2016. DOI: 10.1016/j.ymssp.2015.06.026.
[12] Z. Yang, A. Erturk, and J. Zu, On the efficiency of piezoelectric energy harvesters, Extrem. Mech. Lett., vol. 15, pp. 26–37, 2017. DOI: 10.1016/j.eml.2017.05.002.
[13] E. Brusa, Design of a kinematic vibration energy harvester for a smart bearing with piezoelectric/magnetic coupling, Mech. Adv. Mater. Struct., vol. 27, no. 15, pp. 1322–1330, 2020. DOI: 10.1080/15376494.2018.1508795.
[14] D. Benasciutti, L. Moro, S. Zelenika, and E. Brusa, Vibration energy scavenging via piezoelectric bimorphs of optimized shapes, in, Microsyst. Technol., vol. 16, no. 5, pp. 657–668, 2010. DOI: 10.1007/s00542-009-1000-5.
[15] M. Askari, E. Brusa, and C. Delprete, Design and modeling of a novel multi-beam piezoelectric smart structure for vibration energy harvesting, Mech. Adv. Mater. Struct., vol. 29, no. 28, pp. 7519–7541, 2022. DOI: 10.1080/15376494.2021.2001122.
[16] M. Askari, E. Brusa, and C. Delprete, Vibration energy harvesting via piezoelectric bimorph plates: an analytical model, Mech. Adv. Mater. Struct., vol. 30, no. 23, pp. 4764–4785, 2023. DOI: 10.1080/15376494.2022.2104975.
[17] S.X. Long, S.Y. Khoo, Z.C. Ong, M.F. Soong, Y.H. Huang, N. Prasath, and S. Noroozi, A comprehensive review on mechanical amplifier structures in piezoelectric energy harvesters, Mech. Adv. Mater. Struct., vol. 31, no. 25, pp. 7244–7273, 2024. DOI: 10.1080/15376494.2023.2243674.
[18] X. Zhang, X. Huang, and B. Wang, A quad-stable nonlinear piezoelectric energy harvester with piecewise stiffness for

broadband energy harvesting, Nonlinear Dyn., vol. 112, no. 22, pp. 19633–19652, 2024. DOI: 10.1007/s11071-024-10077-0.
[19] M. Rajarathinam, M. Aravindan, V. Vinothkrishnan, and S.F. Ali, Coupled piezo-multiple electromagnetic energy harvesting, Mech. Adv. Mater. Struct., vol. 30, no. 23, pp. 4882–4901, 2023. DOI: 10.1080/15376494.2022.2107742.
[20] Y. Zhu, S. Duan, Z. Zhang, and P. Zhang, Noncontact magnetically coupled piezo-electromagnetic rotary energy harvester, Mech. Adv. Mater. Struct., pp. 1–14, 2024. DOI: 10.1080/15376494.2024.2394630.
[21] S. Roundy, E.S. Leland, J. Baker, E. Carleton, E. Reilly, E. Lai, B. Otis, J.M. Rabaey, P.K. Wright, and V. Sundararajan, Improving power output for vibration-based energy scavengers, IEEE Pervasive Comput., vol. 4, no. 1, pp. 28–36, 2005. DOI: 10.1109/MPRV.2005.14.
[22] Y. Yang, and L. Tang, Equivalent circuit modeling of piezoelectric energy harvesters, J. Intell. Mater. Syst. Struct., vol. 20, no. 18, pp. 2223–2235, 2009. DOI: 10.1177/1045389X09351757.
[23] Y. Tadesse, S. Zhang, S. Priya, Multimodal energy harvesting system: piezoelectric and electromagnetic, J. Intell. Mater. Syst. Struct., 520 (2009). 625–632. DOI: 10.1177/1045389X08099965.
[24] D. Upadrashta, and Y. Yang, Trident-shaped multimodal piezoelectric energy harvester, J. Aerosp. Eng., vol. 31, no. 5, pp. 04018070, 2018. DOI: 10.1061/(ASCE)AS.1943-5525.0000899.
[25] V.J. Caetano, and M.A. Savi, Multimodal pizza-shaped piezoelectric vibration-based energy harvesters, J. Intell. Mater. Syst. Struct., vol. 32, no. 20, pp. 2505–2528, 2021. DOI: 10.1177/1045389X211006910.
[26] R.M. Toyabur, M. Salauddin, and J.Y. Park, Design and experiment of piezoelectric multimodal energy harvester for low frequency vibration, Ceram. Int., vol. 43, pp. S675–S681, 2017. DOI: 10.1016/j.ceramint.2017.05.257.
[27] H. Deng, Y. Du, Z. Wang, J. Zhang, M. Ma, and X. Zhong, A multimodal and multidirectional vibrational energy harvester using a double-branched beam, Appl. Phys. Lett., vol. 112, pp. 143902, 2018.
[28] P.-D. Mitcheson, T.-C. Green, and E.-M. Yeatman, Power processing circuits for electromagnetic, electrostatic and piezoelectric inertial energy scavengers, Microsyst. Technol., vol. 13, no. 11-12, pp. 1629–1635, 2007. DOI: 10.1007/s00542-006-0339-0.
[29] C.R. Bowen, P.F. Giddings, A.I.T. Salo, and H.A. Kim, Modeling and characterization of piezoelectrically actuated bistable composites, IEEE Trans. Ultrason. Ferroelectr. Freq. Control., vol. 58, no. 9, pp. 1737–1750, 2011. DOI: 10.1109/TUFFC.2011.2011.
[30] Designerdata, n.d. Available: https://designerdata.nl/materials/plastics/thermo-plastics/polyamide-6.6. Accessed: Sep. 6, 2024.
[31] D.S. Ibrahim, S. Beibei, S. Fatai, O.A. Oluseyi, and U. Sharif, Numerical and experimental study of a gauge-shaped beam for improved performance of piezoelectric energy harvester, Microsyst. Technol., vol. 27, no. 12, pp. 4253–4268, 2021. DOI: 10.1007/s00542-021-05219-y.
[32] M.W. Hyer, Stress Analysis of Fiber-Reinforced Composite Materials, DEStech Publications, Inc. 439 North Duke Street Lancaster, Pennsylvania 17602 U.S.A., 2009.
[33] S. Roundy, P.K. Wright, and J. Rabaey, A study of low level vibrations as a power source for wireless sensor nodes, Comput. Commun., vol. 26, no. 11, pp. 1131–1144, 2003. DOI: 10.1016/S0140-3664(02)00248-7.
[34] S. Roundy, and P.K. Wright, A piezoelectric vibration-based generator for wireless electronics, Smart Mater. Struct., vol. 13, no. 5, pp. 1131–1142, 2004. DOI: 10.1088/0964-1726/13/5/018.
[35] H.A. Sodano, G. Park, and D.J. Inman, Estimation of electric charge output for piezoelectric energy harvesting, Strain., vol. 40, no. 2, pp. 49–58, 2004. DOI: 10.1111/j.1475-1305.2004.00120.x.
[36] N.E. DuToit, and B.L. Wardle, Experimental verification of models for microfabricated piezoelectric vibration energy harvesters, Aiaa J., vol. 45, no. 5, pp. 1126–1137, 2007. DOI: 10.2514/1.25047.
[37] E. Brusa, A. Carrera, and C. Delprete, A review of piezoelectric energy harvesting: materials, design, and readout circuits, Actuators., vol. 12, no. 12, pp. 457, 2023. DOI: 10.3390/act12120457.
[38] M.S. Mohd Resali, and H. Salleh, Development of multiple-input power management circuit for piezoelectric harvester, J. Mech. Eng., vol. 2, pp. 215–230, 2017.
[39] H.C. Lin, P.H. Wu, I.C. Lien, and Y.C. Shu, Analysis of an array of piezoelectric energy harvesters connected in series, Smart Mater. Struct., vol. 22, no. 9, pp. 094026, 2013. DOI: 10.1088/0964-1726/22/9/094026.
[40] E. Brusa, A. Carrera, and C. Delprete, Integrated mechatronic design of an industrial piezoelectric vibration energy harvester, Mech. Adv. Mater. Struct., vol. 31, no. 27, pp. 8966–8980, 2024. DOI: 10.1080/15376494.2023.2264047.
[41] Y. Zhang, K. Bian, Y. Gu, M. Ye, W. Tian, and W. Liu, Cost-effective and scalable rectifier design for multiple piezoelectric power sources with improved performance, J. Intell. Mater. Syst. Struct., vol. 31, no. 1, pp. 167–181, 2020. DOI: 10.1177/1045389X19888714.
[42] E.L. Pradeesh, and S. Udhayakumar, Effect of placement of piezoelectric material and proof mass on the performance of piezoelectric energy harvester, Mech. Syst. Signal Process., vol. 130, pp. 664–676, 2019. DOI: 10.1016/j.ymssp.2019.05.044.
[43] A.G.A. Muthalif, and N.H.D. Nordin, Optimal piezoelectric beam shape for single and broadband vibration energy harvesting: modeling, simulation and experimental results, Mech. Syst. Signal Process., vol. 54-55, pp. 417–426, 2015. DOI: 10.1016/j.ymssp.2014.07.014.
[44] A. Erturk, P.A. Tarazaga, J.R. Farmer, and D.J. Inman, Effect of strain nodes and electrode configuration on piezoelectric energy harvesting from cantilevered beams, J. Vib. Acoust., vol. 131, pp. 0110101–01101011, 2009.
[45] E. Brusa, F. De Bona, A. Gugliotta, and A. Somà, Modeling and prediction of the dynamic behaviour of microbeams under electrostatic load, Analog Integr. Circuits Signal Process., vol. 40, no. 2, pp. 155–164, 2004. DOI: 10.1023/B:ALOG.0000032596.58984.0c.
[46] E. Brusa, S. Carabelli, F. Carraro, and A. Tonoli, Electromechanical tuning of self-sensing piezoelectric transducers, J. Intell. Mater. Syst. Struct., vol. 9, no. 3, pp. 198–209, 1998. DOI: 10.1177/1045389X9800900306.
[47] M. Askari, E. Brusa, and C. Delprete, On wave propagation and free vibration of piezoelectric sandwich plates with perfect and porous functionally graded substrates, J. Intell. Mater. Syst. Struct., vol. 33, no. 16, pp. 2049–2073, 2022. DOI: 10.1177/1045389X211072195.
[48] FR4 Material Properties - Piezo Support, n.d. Available: https://support.piezo.com/article/62-material-properties. Accessed: Sept. 24, 2024.
[49] M. Yuan, Z. Cao, and J. Luo, Characterization of the influences of diodes on piezoelectric energy harvester, Int. J. Smart Nano Mater., vol. 9, no. 3, pp. 151–166, 2018. DOI: 10.1080/19475411.2018.1454532.

Appendix

The material properties of PZT-5A and PZT-5H are provided in Table A1, and the read-out circuits, simulated in LTspice, are illustrated in Figure A1.

Table A1. Mechanical and electrical properties of PZT materials.

Properties	PZT-5A	PZT-5H
Elastic moduli (GPa)		
C_{11}	99.2	127.2
C_{12}	54.0	80.2
C_{33}	86.9	117.4
C_{13}	50.8	84.7
C_{55}	21.1	23.0
C_{66}	22.6	23.5
Dielectric moduli (nF/m))		
$\in_{11}^{\sigma}$	15.3	15.1
$\in_{33}^{\sigma}$	15.0	12.7
Piezoelectric moduli (C/m^2)		
e_{31}	−7.2	−6.6
e_{33}	15.1	23.2
e_{15}	12.3	17.0
Density (kg/m^3)		
ρ	7750	7500

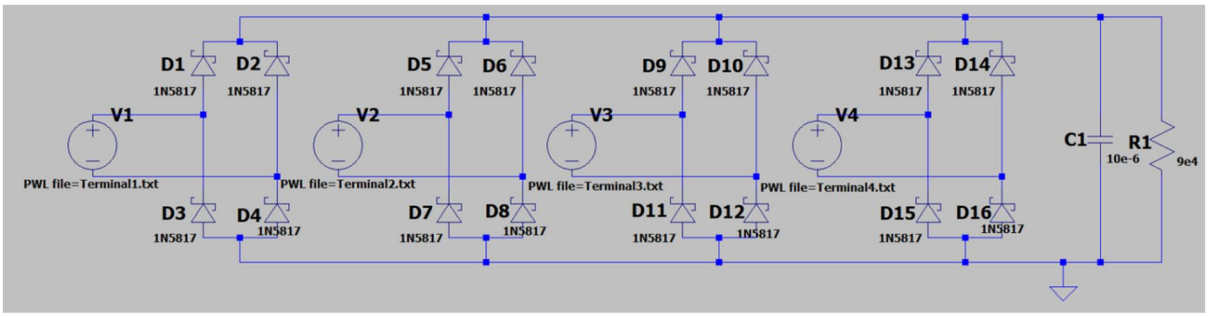

(a)

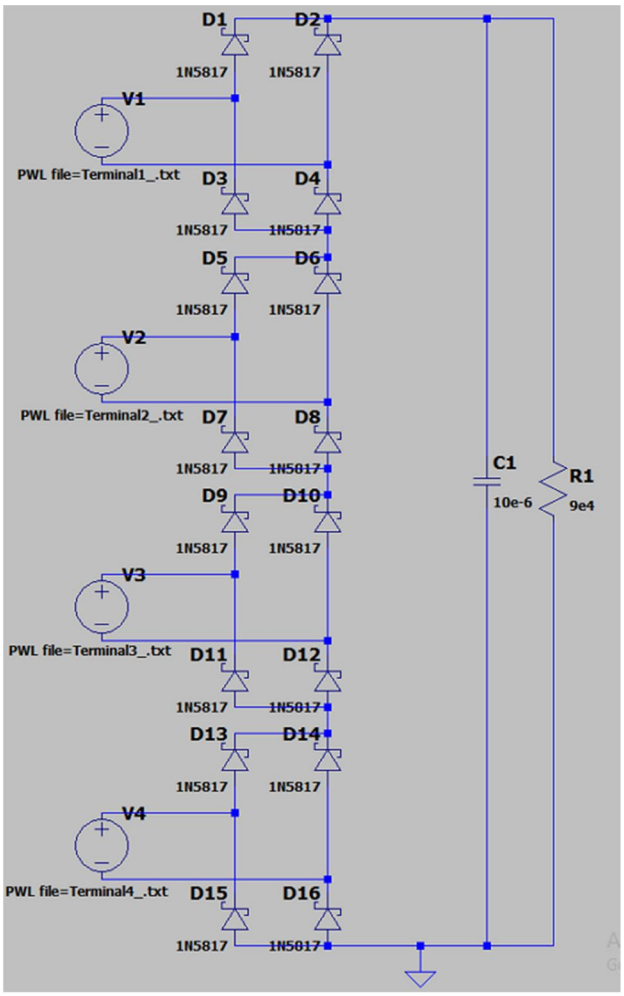

(b)

Figure A1. Read-out circuit simulated in LTspice (a) parallel configuration (b) series configuration.